Investigation of applying grid-forming converter control on wind turbines and its influence on power systems

Master of Science Thesis
Aalborg University
Department of Energy Technology
2020

Nikolaj Stig Stoltenborg

AALBORG UNIVERSITY

SIEMENS Gamesa
RENEWABLE ENERGY

Energy Technology
Aalborg University
http://www.et.aau.dk

AALBORG UNIVERSITY
STUDENT REPORT

Title:
Investigation of applying grid-forming converter control on wind turbines and its influence on power systems

Project Period:
Master's Thesis spring 2020

Project Group:
EPSH4-1031

Participant(s):
Nikolaj Stig Stoltenborg

Supervisor(s):
Jayakrishnan Radhakrishna Pillai
Sanjay Chaudhary

Copies: 1

Page Numbers: 72

Date of Completion:
29-05, 2020

Abstract:

The instantaneous penetration level of RES is expected to increase in the future. This is expected to raise new power system stability challenges, as conventional SGs will be replaced with converter based power sources. The grid-forming converter (GFC) control concept is anticipated to possess the required capabilities to overcome the expected power system challenges. This project investigates the characteristics of GFCs, together with the considerations of applying GFC control to WTGs. A dynamic RMS model is developed in DIgSILENT PowerFactory to represent an aggregated wind farm with GFC control. The developed GF model is utilised to investigate power system support offered by a wind farm operating in GF mode. The GF model was compared to a conventional SG and an aggregated wind farm model. It was found that the GF model could offer similar system support compared to an SG. However, converter based grid-forming units have unlike SGs a strict operation boundary owing to hardware limitations. Moreover, it was found that the GF model could outperform SGs in some areas, as a converter based grid-forming units have more extensive parameter design freedom compared to conventional SGs.

Preface

This report is written by EPSH4-1031 on the 4^{th} semester of the master's degree, High Voltage and Power System Engineering at Aalborg University. The project was made under the supervision of Jayakrishnan Radhakrishna Pillai and Sanjay Chaudhary from Aalborg University.

I owe a special thanks to my contact person Thyge Knueppel from Siemens Gamesa Renewable Energy and the Grid Compliance team at Siemens Gamesa, which have been excellent in giving support, comments and guidance throughout the project period.

Nikolaj Stig Stoltenborg

Readers' guide

The literature used in the project consists of web pages, books, reports and academical papers. A combined list with details of the sources used in the project can be found in the Bibliography. A numeric system, based in IEEE citation style, is used for citation. Thus, the presented sources have been assigned a digital number by order of appearance. Figures, Tables, and Equations are likewise numbered per its debut in the text.

The developed DIgSILENT PowerFactory model, together with the test system presented in the project, can be found in the zip folder attached to the report.

Contents

Nomenclature

Abbreviations

AC	Alternating Current
CE	Continental Europe
DC	Direct Current
DSL	Dynamic Simulation Language
EMF	Electromotive Force
$ENTSO-E$	European Network Transmission System Operator for Electricity
GB	Great Britain
GBC	Generator Bridge Converter
GFC	Grid-forming Converter
GVA	Giga Voltage Ampere
$IBPS$	Inverter-Based Power Source
MVA	Mega Voltage Ampere
MW	Mega Watt
NBC	Network Bridge Converter
PLL	Phase Lock Loop
pu	Per Unit
PV	Photovoltaic
PWM	Pulse Width Modulation
RES	Renewable Energy Source
RMS	Root Mean Square
$RoCoF$	Rate of Change of Frequency
SC	Synchronous Condenser

SG	Synchronous generator	
SM	Electromagnetic transients	
SM	Synchronous Machine	
TSO	Transmission System Operator	
VSM	Virtual synchronous machine	
WTG	Wind Turbine Generator	

Electrical notation

β	Frequency bias	[W/Hz]
$\Delta\omega_r$	Rotor speed deviation	[1/s]
ΔE	Energy	[J]
ΔP_{Load}	Load power	[W]
δ	Power angle	[-]
ω	Rotor frequency	[1/s]
ω_g	Grid frequency	[1/s]
ω_n	natural frequency	[1/s]
ω_{0m}	Rated angular velocity of rotor	[1/s]
ω_0	Electrical synchronous speed	[1/s]
ρ	Active power droop gain	[-]
τ_{acc}	accelerating torque	[Nm]
τ_{el}	electrical torque	[Nm]
τ_{mech}	Mechanical torque	[Nm]
ζ	Damping ratio	[-]
E	Internal converter voltage	[pu]
f_0	nominal frequency	[Hz]
f_{ref}	Frequency reference	[pu]
H	Inertia constant	[s]
I_{max}	Maximum converter current	[pu]

J	Combined moment of inertia	$[Kg \cdot m^2]$
K_D	Damping factor	[pu torque/pu speed deviation]
K_s	Synchronising power coefficient	[-]
m_p	Active power effective gain	[-]
m_q	Reactive power droop gain	[-]
P_{rated}	Rated active power	[W]
S_n	Rated power	[VA]
SCR	Short circuit ratio	[-]
Sk''_{max}	Short circuit power	[VA]
T_a	Acceleration time constant	[s]
V_t	Terminal voltage	[pu]
V_{ref}	Voltage reference	[pu]
Z_{filter}	Filter impedance	[pu]

Chapter 1

Introduction

Background analysis

Today the European electrical power system contains approximately 39% renewable energy sources (RES). However, it is anticipated that the European power system will accommodate an increasing amount of RES in the future [1]. The majority of the predicted increase of RES will be non-synchronous generators (NSGs) like wind and solar, which are typically inverter-based power sources (IBPSs) [2]. With the increasing amount of RES in the future, fewer conventional synchronous generators (SGs) are assumed to be connected to the power system.

The electrical power system was developed based on large synchronous generators and the dynamic and steady-state properties from these synchronous generators. Hence, replacing SGs with IBPSs can create new system challenges. [3]

The transmission system operators (TSO) in Ireland and Great Britain have anticipated, that a tipping point exists for the penetration level of IBPS in the electrical power system. The tipping point defines the maximum share of IBPS for which the remaining synchronous generators cannot provide sufficient system response and mitigate the effect of introducing additional IBPS to the power system. The tipping point is estimated to be 65%. [4] [3]

The power system in areas such as South Australia, Tasmania, Texas, Hawai and Ireland are experiencing instantaneous penetration levels of IBPSs in the range of 50-60% [5]. The European Network of Transmission System Operators for Electricity (ENTSO-E) has conducted a forecast of the highest RES penetration level in any hour in the year 2025 for each European country. The forecast is displayed in Figure 1.1.

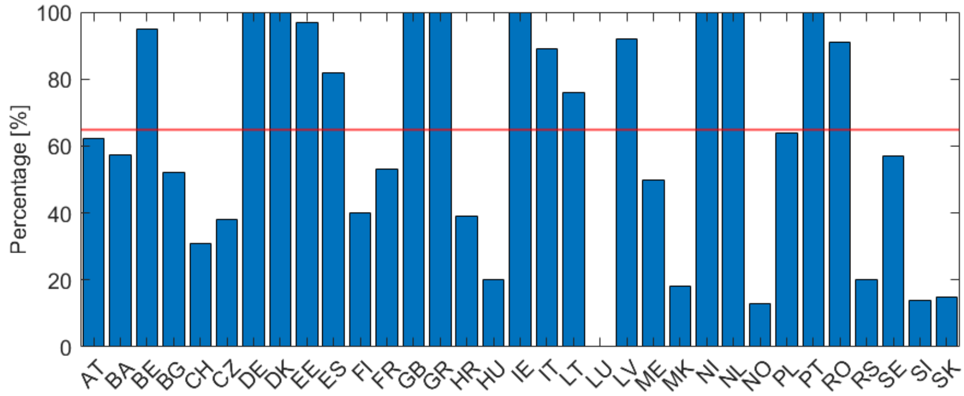

Figure 1.1: Highest penetration level of RES in any hour in Europe by 2025. [1]

From Figure 1.1, it can be concluded that 15 countries in Europe will experience a penetration level of RES above 65% by 2025.

Furthermore, ENTSO-E has also predicted the penetration level of RES by 2025 for different synchronous areas in Europe. The data used for the prediction is based on ENTSO-E Ten Year Development Plan [1]. The predicted penetration level for Continental Europe (CE) and Great Britain (GB) is arranged as duration curves and shown in Figure 1.2.

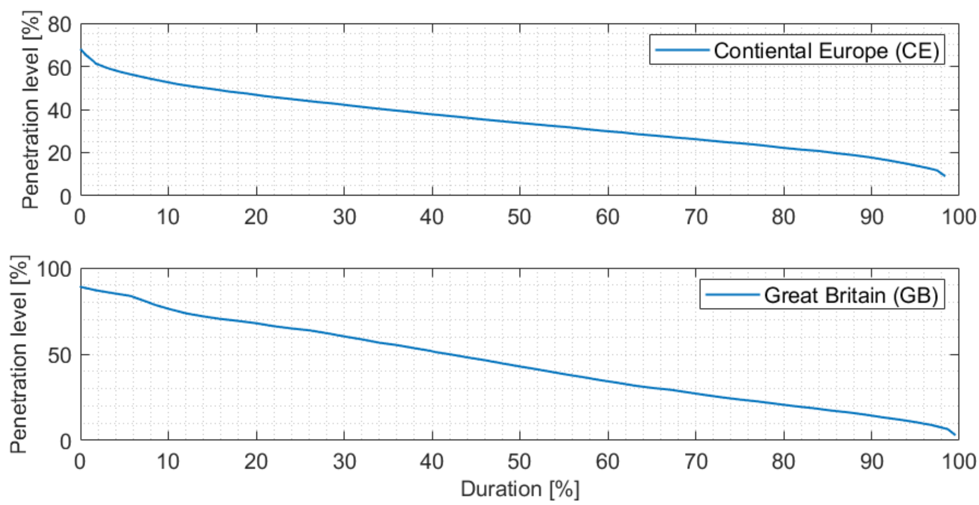

Figure 1.2: Duration curve of percentage of RES in CE and GB during a period of one year in 2025. [1]

From Figure 1.2, it can be seen that Continental Europe is estimated to experience a penetration level of RES above 65% in approximately 1% of the time, by 2025. However, considering the duration curve of GB, it can be seen that the penetration level of RES is estimated to exceed 65% in approximately 24% of the time, during the year 2025. [2]

The presented data in Figure 1.1 and Figure 1.2 consider the RES penetration level. It should be noted that RES's will represent not only IBPS's but also synchronous generators, like hydro and biofuel plants. However, some countries have already started to substitute IBPSs with SGs at certain times to ensure the power system stability. A report from National Grid ESO showed that in 2018 £150M was spend in Great Britain on substituting RES with SGs and that this cost is estimated to increase in the future rapidly. [2] Therefore, it is essential to explore alternative solutions to allow a higher penetration level of RES.

Analysis of potential technologies to allow a higher penetration level of RES

As demonstrated in the *Background analysis*, the share of IBPS's is expected to increase in the future. This implies that the penetration level of SGs will be diminished as RES can often produce energy at a lower cost than SGs. However, the dynamic properties of SGs are required to maintain a stable power system, as will also be introduced in Section 2.1. Henceforth, this section will briefly present and discuss the potential technologies which can deliver a similar dynamic response as SGs.

National Grid has made a study to evaluate different potential technologies to enable the estimated increasing penetration level of RES. The evaluation is summaries in Figure 1.3.

National Grid's evaluation in Figure 1.3 is based on a list of critical capabilities which should be maintained in power systems. The critical capabilities are identified in different published journals [4] [6] [7]. However, these capabilities must be adequately delivered to power systems to ensure system stability. In addition to the evaluation of the defined critical capabilities in Figure 1.3, the potential cost and maturity of the different technologies are also ranked by National Grid.

From Figure 1.3, it is shown how only the first three technologies from the top can offer a potential holistic solution to all the identified critical capabilities. Technologies which offer a holistic solution are often desirable by TSO's since the potential risk is associated with treating the different critical capabilities individually. E.g. a solution to one of the critical capabilities can lead to deterioration of another. [2]

Solution	Estimated Cost	RoCoF [*] [2]	Sync Torque/Power (Voltage Stability/Ref) [2] [3] [4]	Prevent Voltage Collapse [2]	Prevent Sub-Sync Osc. / SG Compitable [2] [3]	Hi Freq Stability [2]	RMS Modelling [*] [2] [3] [4]	Fault Level [*] [2]	Post Fault Over Volts [2]	Harmonic & Imbalance [5]	System Level Maturity	Notes
Constrain Asyncronous Generation	Hgh	I	Yes	Yes	Yes	Yes	Yes	Yes	Yes	Yes	Proven	These technologies are or have the potential to be Grid Forming / Option 1
Syncronous Compensation or More Sync. Gens at lower load	High	I	Yes	Yes	Yes	Yes	Yes	Yes	Yes	Yes	Proven	
VSM	Medium	Yes	Yes	Yes	Yes	Yes	Yes	Yes	Yes	P	Modelled	
VSM0H	Low	No	Yes	Yes	No	P	P	P	Yes	P	Modelled	Has the potential to contribute but relies on the above Solutions
Synthetic Inertia	Medium	Yes	No	No	P	No	No	No	No	No	Modelled	
Other NG Projects	Low	Yes	P	Yes	No	No	No	P	P	No	Theoretical	

Key
No — Doesn't Resolve Issue
P I — Potential Improves
Yes — Resolves Issue

Figure 1.3: Evaluation conducted by National Grid of alternative technologies to deliver synchronous generators dynamic properties [6]

The first solution, from Figure 1.3, is to deal with the listed critical capabilities is to constrain or curtail the production of asynchronous generations online, which is often RES, below the tipping point. This approach is estimated to cost in the range of 3-4£B per year in the year 2030 [6]. Thus, this will be an unacceptable approach to pursue in the distant future.

The second technical solution, from Figure 1.3, is the use of synchronous condensers (SC). SC is today the most common way to deal with the listed critical capabilities, especially to enhance system strength.

A case study was made for GB to explore the capability of installing SCs, to obtain power system stability for a 100% non-synchronous power system. It showed that more than 10 GVA of SCs was required to cover the critical capabilities which arise with a 100% non-synchronous power system [2]. Thus, utilising SCs will present an expensive solution for smaller synchronous regions like Ireland and GB. [7]

The third technical solution, virtual synchronous machine (VSM), from Figure 1.3, will also undertake a holistic solution to the listed critical capabilities and is indicated to be cheaper than the two other solutions. VSM is a control concept, that can be implemented on IBPS, which will enable traditional gird-following units, like WTGs and PVs, to act as a grid forming unit, like SGs. Note, VSM is just representing one approach to achieve grid-forming behaviour for an IBPS. Thus, gird-forming converters (GFC) will represent a more generic definition. Different GFC concepts will be presented in Section 2.4.

An extensive research project, involving 11 European TSO's, called MIGRATE, which is funded from the European Union's Horizon 2020 research and innovation fund has initiated the investigation of the GFC technology as a potential solution to replace SGs in power systems. [8] [9][10]

This have started a natural response by RES manufactures to explore their technologies capability of offering a version of GFC support. General Electric Research has recently announced that they are investigating the opportunities of operating PV inverters to offer system support [11]. SMA is currently offering off-grid battery inverters [12]. Siemens Gamesa has already carried out a trial over eight weeks, where 23 turbines were equipped with a grid supporting control [13].

Problem formulation

From the established background analysis, it will be relevant to investigate how WTGs, operated with grid-forming converter control, can enhance power system stability and assist the replacement of SGs in the future. Thus, the scope of this project is to investigate how a grid-forming model can be developed to represent WTGs with grid-forming converter control and how this model can be used to analyse the influence of implementing WTGs with grid-forming control on power systems.

Objectives

This project aims to analyse the effect of applying grid forming converter control to WTGs and investigate its advantageous in power systems operation. It is accomplished through the following objectives.

- What are the characteristics and working principle of grid-forming power converters?
- What design properties and constraints does grid-forming converter controlled WTGs have?
- How can a dynamic simulation model of WTGs be developed to provide the characterises of grid-forming power converters?
- How will WTGs contribute to power systems when controlled as a grid-forming power unit compared to conventional SGs and WTGs?

Delimitation

Some limitations are made for this project. These limitations are listed below:

- Only the full-scale converter type WTG has been considered for the implementation of grid-forming converter control.
- The dynamic grid-forming model is developed as an aggregated model to represent a wind farm and not a single WTG. Thus, the dynamic behaviour of a WTG's generator and generator bridge converter is not analysed.
- The grid-forming model is conducted without considering the dynamics of wind power curves, shaft and blade angle control.

- The dynamic grid-forming model is developed in DIgSILENT PowerFactorys RMS domain, where only the positive sequence components are utilised. Hence, the harmonic contribution and transient behaviour of the grid-forming model is not analysed.

Methodology

This section will elaborate on which methods are used to answer the listed objectives of this project. Moreover, it will be explained how the presented results are evaluated.

A state of the art analysis is conducted to investigate different grid-forming converter control typologies. The state of the art analysis is based on a thorough literature-review based on published academic papers.

A dynamic model is developed to represent an aggregated wind farm operating in grid-forming mode. The model is developed based on the state of the art analysis of GFCs. The dynamic model, is developed in the simulation software DIgSILENT PowerFactory with the utilisation of PowerFactory's dynamic simulation language (DSL). Time-varying simulations are used to test the individual response of the control blocks developed for the dynamic grid-forming model. The test response is then verified against mathematical equations.

To evaluate the overall response of the developed dynamic GF model, an SG and a WTG model are implemented from PowerFactory's dynamic models' library. Time-varying simulations are further utilised to test and compare the power system contribution from the three power units.

Success criteria

The success criteria of this project are to develop a grid-forming model, which can be used to represent an aggregated wind farm equipped with grid forming converter control. The grid-forming model should be able to operate in parallel in flexibly with other power system units. With the grid-forming model developed, it should be possible to test and validate the influence of a GFC on a given power system, owing to different system disturbances.

Outline of the report

The outline of the project consists of four chapters. Each chapter is organised as follows:

Chapter 2 - Technical background: In this chapter, a literature review is conducted to develop an understanding of the technical background of the conventional SGs and WTGs power unit together with a state of the art investigation of grid forming converter control concepts. Lastly, some relevant considerations are introduced for GFC control applied to WTGs.

Chapter 3 - Development of grid-forming WTG model: In this chapter, a dynamic grid-forming model is developed in DIgSILENT PowerFactory to represent an aggregated wind farm. Moreover, a test system is created in PowerFactory to evaluate the behaviour of the different blocks of the grid-forming model.

Chapter 4 - Grid-forming WTG model compared to SGs and WTGs: In chapter 4, the contribution of the grid-forming model is compared to a conventional SG and WTG model. The three generation units are implemented into a test system, where different system disturbances are applied. This is done to evaluate the contribution from the three generators and their effect on power systems.

Discussion, Conclusion & Future work: Lastly, the main findings of the project are discussed. Furthermore, the main conclusions of the project are presented together with suggestions for future work.

Chapter 2

Technical background

This chapter contains a short classification of classical power system stability, a general review of the control of SGs and full-scale converter wind turbines. Furthermore, state of the art of grid-forming converter control concepts is presented. Lastly, the physical and practical constraints related to applying grid-forming converter control to wind turbines are introduced.

2.1 Power system stability

Power system stability is defined by the ability of a power system to recover to an equilibrium state upon being subjected to a system disturbance. In general, power system stability can be divided into three stability categories which are, rotor angle, frequency and voltage stability. This will allow a more straightforward quantification of power system stability. Figure 2.1 displays the three categories.

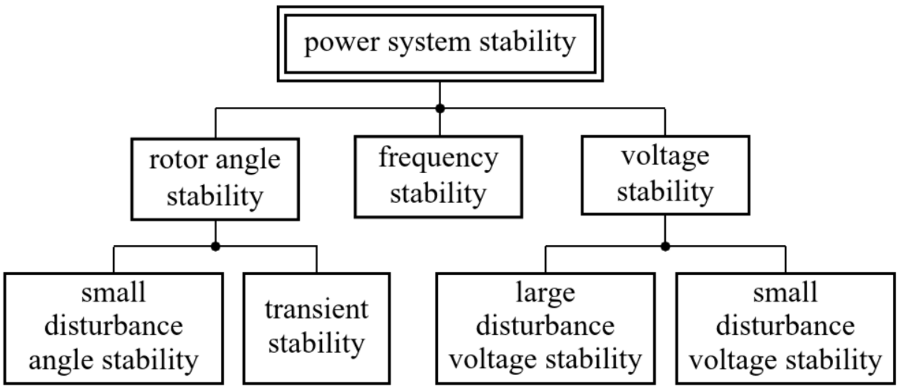

Figure 2.1: Classification of power system stability [14]

Rotor angle stability is referred to as the angles of nodal voltages (δ) in a power system. It is an expression of the ability of interconnected synchronous machines in a power system to remain synchronised. There exists a strict correlation between the output power and the rotor angle of a synchronous machine. The correlation is highly non-linear. Thus, beyond a certain rotor angle, an increase in the rotor angle will lead to a decrease in power transfer, which in turns leads to a further increase in the rotor angle and thus instability is met.

Frequency stability is an expression of the ability of a power system to maintain a steady-state frequency within a specified nominal range after being subjected to a substantial imbalance between generation and load. An imbalance is usually associated with a massive load suddenly being connected or disconnected to a power system, or a large generator, that is suddenly disconnected. In such cases, the frequency response can be divided up into four categories. The four categories are inertia response, primary response, secondary response and tertiary response. The inertia response is typically within a few seconds. The primary response is typically up to a few minutes. The secondary response and tertiary response is typically up to 30 minutes or more. If control of the four categories is not done correctly, the system frequency will not recover, and it can ultimately lead to system collapse.

Voltage stability is defined as the ability of a power system to maintain steady acceptable voltage magnitudes at all nodals in a power system. The main circumstance which creates voltage instability is the inability of a power system to oblige the reactive power demand. A system is voltage stable, if the bus voltage magnitude increases as the reactive power injected at the same bus increase. Contrary, a system is voltage unstable, if the bus voltage magnitude decreases as the reactive power injected at the same bus increases.

The voltage stability can further be classified into large -and small disturbances. Large disturbance voltage stability is defined as a system's ability following a large system event, such as system fault or loss of a large generator, to control the voltages. Small disturbance voltage stability is defined as a system's ability following small incremental changes in system load to control the voltages.

2.2 General operation of synchronous generators

A synchronous generator (SG) will typically have a prime mover which is controlled by a governor controller. The governor is controlling the valves, which allows an increase or decrease in mechanical power generator by the turbine. The stator voltage magnitude of an SG is controlled by a field excitation system. From the excitation system, it is possible to control the reactive power contribution from an SG.[14]

If an unbalance between the mechanical torque, and the electrical torque of an SG exists, swings can be created, which are essential for power system oscillation studies. This swing can be described with Equation (2.1).

$$\tau_{acc} = \tau_{mech} - \tau_{el} = J\frac{d\omega_m}{dt} \tag{2.1}$$

Where, τ_{acc} is the accelerating torque, τ_{mech} is the mechanical torque, τ_{el} is the electrical (electromagnetic) torque. From Equation (2.1) it can be seen that if $\tau_{mech} > \tau_{el}$, then τ_{acc} is positive and the rotor accelerates and conversely if $\tau_{mech} < \tau_{el}$ then τ_{acc} is negative and the rotor decelerates. The acceleration and deceleration of a rotor can be described by the combined inertia of a generator, as a consequence of the rotating mass of a rotor. In Equation (2.1), J describes the combined moment of inertia where ω_m is the angular velocity of the rotor. The combined moment of inertia can be mathematically described by Equation (2.2).[15]

$$J = \frac{2HS_n}{\omega_{0m}^2} \tag{2.2}$$

Where S_n is the rated power of an SG, ω_{0m} is the rated angular velocity of the rotor and H is the inertia constant. The inertia constant, H, of a generator can be determined from the seconds it will take the generator to provide the same amount of energy, as stored in the rotor, when the generator is operated at its rated MVA power. [6][14]

From Equation (2.2) and Equation (2.1) is possible to obtain the classical swing equation in per-unit form, where a damping term proportional to the speed deviation it added. It is shown in Equation (2.3). Note, the angular velocity in Equation (2.3) is expressed in electrical instead of mechanical rad/s. [15][14]

$$\frac{2H}{\omega_0} \cdot \frac{d^2\delta}{dt^2} = T_{mech} - T_{el} - \frac{K_D}{\omega_0}\frac{d\delta}{dt} \tag{2.3}$$

Where T_{mech} and T_{el} is the per-unit mechanical and electrical torque, respectively. ω_0 is the rated electrical angular velocity, δ is the rotor angle in electrical degrees and K_D

is the damping coefficient. The last term in Equation (2.3) is describing the damping torque of an SG. The damping torque of an SG is designed to help the generator reach equilibrium faster after being subjected to a rotor speed disturbance. Thus, only in a transient state, if the rotor speed is not equal to the synchronous speed an electromotive force (emf) is induced in the damping windings of an SG.

Equation (2.3) can also be expressed from two first-order differential equation as in Equation (2.4) and Equation (2.5).

$$\frac{d\Delta\omega_r}{dt} = \frac{1}{2H}(T_{mech} - T_{el} - K_D\Delta\omega_r) \tag{2.4}$$

$$\frac{d\delta}{dt} = \omega_0\Delta\omega_r \tag{2.5}$$

The time derivative of the rotor angle can be expressed from the angular rotor speed deviation ($\Delta\omega_r = \omega_{rotor.velocity} - \omega_0$). From Equation (2.4), it can be seen that large inertia (H) will limit the magnitude of $d\Delta\omega_r/dt$, which is equivalent to the rate of change of frequency (RoCoF). Thus, SGs will inherently support frequency stability from the kinetic energy stored in the rotating mass of the rotor.[15][14]

2.3 General operation of full-scall wind turbine converters

An control diagram of a full scale converter type wind turbine, is displayed in Figure 2.2.

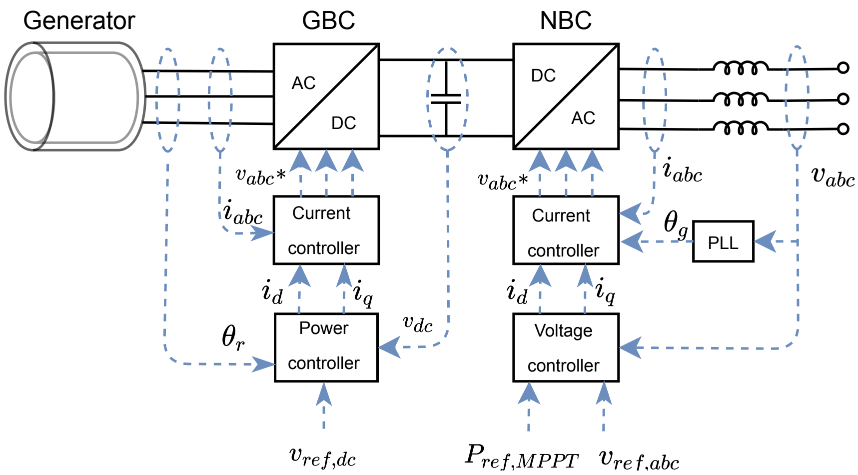

Figure 2.2: An electrical and control schematic of a full-scale wind turbine. The blue dashed lines are control/measurement signals. GBC is the machine-side converter and NBC is the grid-side converter. [16]

From Figure 2.2, the electrical layout of a full-scale converter wind turbine consists of a generator, a generator-bridge AC/DC converter (GBC), a DC link with a shunt capacitor and a network-bridge DC/AC converter (NBC). In the control scheme presented in Figure 2.2, the active power output is adjusted by the NBC, and the DC link voltage is adjusted by the GBC. [17] [16]

The GBC is controlled by two control loops, an inner and an outer. The outer loop controls the DC link voltage by comparing the measured DC voltage v_{dc} to the reference dc voltage $v_{ref,dc}$. The inner loop gets reference values from the outer loop. The inner loop controls the d -and q axis component in the GBC. [16]

The current flowing into the DC-link capacitor from the GBC must be equal to the current flowing out of the DC-link capacitor to the NBC when converter losses are neglected. It is done to maintain that the DC-link voltage constant in steady-state conditions. The current drawn from the DC-link capacitor is ensured by the NBC. [16][17]

The NBC is also controlled by two control loops, as shown in Figure 2.2. The outer loop is utilised to control the active power injected to the grid. This is achieved with a maximum power point tracker, $P_{ref,MPPT}$, which is calculated based on the measured wind velocity or rotor speed. The outer loop is also utilised to control the reactive power flow. It is done by controlling the AC voltage magnitude of the converter. The slow outer loop creates d -and q current axis references to the inner control loop. [17]

The inner control loop is controlled to reach the current reference values determined by the outer loop. The current loop then outputs a voltage reference which is converted to PWM signals and sent the the power modules of the converter. A phase lock loop (PLL) is utilised to synchronise the converter to the AC grid. The PLL measures the voltage phase angle of the AC grid, which is used to create a dq reference system.

WTGs converters are referred to as grid-following converters. This means the converters require a stable voltage reference for the PLL, to measure the voltage phase angle to inject the desired active and reactive power. Hence, wind turbine converters follow the grid frequency instead of controlling the frequency output. [10] [9]

The generator and the mechanical rotating mass of a full-scale converter wind turbine is fully decoupled from the grid. It means, inherently a full-scale wind turbine does not provide the same oscillatory response to disturbances as SGs.

2.4 Grid-forming converter control concepts

Different grid-forming converter control concepts have been proposed for the last decade. However, GFC applications have mainly been used in microgrids so far, and have not been rolled out as substantial as grid-following converts, which is the most typical converter control concept today for RES manufactures. As a consequence, the expected services and capabilities of GFC are still not fully defined by TSO's. However, ENTSO-E has in a working group with the industry defined a list of desired capabilities of grid-forming converters. The capabilities are: *create system voltage, contribute to fault level, contribute to total system inertia (TSI), support system survival, prevent adverse control system interactions, act as a sink to harmonics in the voltage system, act as a sink to unbalance in system voltage [1].* [2][18][3]

These capabilities can be offered by a voltage source. Thus, grid-forming converters should behave like a voltage behind an impedance with a slowly modulated frequency phase and magnitude in order to fulfil ENTSO-E's working groups defined capabilities of a grid forming converter. It implies the current from the grid-forming unit is determined from the load and network condition, which allows the current to change quickly. [1][19]

This section will present some of the different grid-forming converter control concepts. In general, GFCs can be classified into a top level control method and low level control method. Table 2.1 presents an overview of different GFC types with their possible top level and low level converter control methods. [20]

Table 2.1: Classification of grid-forming converter control methods

Top level control	Low level control/Converter interface			
	Voltage reference (Direct PWM)	Voltage reference (Cascaded control)	Current reference (Hysteresis control)	Power reference (Current control)
VSM	✓	✓	✓	✗
Inertia emulation	✗	✗	✗	✓
Voltage injection concept	✗	✓	✗	✗
Droop control	✓	✓	✓	✗

From Table 2.1, four top level control categories are presented and referred to as:

- Virtual Synchronous Machines (VSM)
- Inertia emulation
- Voltage injection concept
- Droop controlled

The low-level control or the interface control to a converter can be further classified into four categories. These four categories are referred to as Voltage reference direct PWM, Voltage reference cascaded control loops, Current reference hysteresis control and Power reference current control. [20]

The different GFC controls from Table 2.1 will be presented and elaborated below.

2.4.1 Virtual Synchronous Machines

The VSM top level control, emulate the essential dynamic behaviours of a real synchronous machine (SM) to the control of a power electronic converter. Hence, to implement the inherent power system stability advantages of SMs, as described in Section 2.2. It is achieved by implementing a mathematical model of SM dynamics to the control system of a converter. [20]

The complexity and accuracy of SM models for VSM vary. Some technical articles utilise 5th and 7th order models of SM. However, it is a common practice for VSM to emulate the inertia and damping response of SMs since these are the two main desirable features for power system stability. [20] These features can be achieved from the classical swing equation, which was presented in Equation (2.4). The swing equation can be expressed more conveniently by replacing the torque terms with power. This can be done by multiplying the torque with the rotor frequency, ω. The swing equation expressed in terms of power can be seen in Equation (2.6). The mechanical power is replaced with an emulated mechanical power, P_0. [20]

$$\frac{d\Delta\omega_r}{dt} = \frac{1}{2H}(P_0 - P_{el} - K_D(\omega - \omega_g)) \tag{2.6}$$

From the swing equation, the control structure can be implemented as a block diagram, as shown in Figure 2.3. The virtual rotor angle of the VSM, $\theta*$, is derived from the

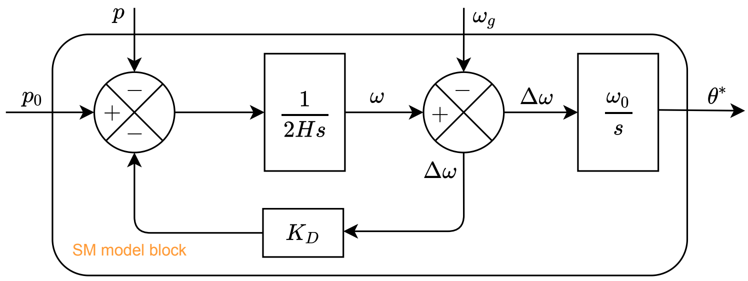

Figure 2.3: Block diagram of SM model based on swing equation shown in Equation (2.6)

integral of the virtual rotating speed of the machine, ω. The virtual rotor angle position is equal to the phase angle of the induced voltage by the VMS model. In [20], it is proposed to decouple the voltage amplitude injected by the VSM or reactive power from the inertia emulation. It can be done by a reactive power droop controller as can be described by Equation (2.7)

$$v^* = v_0 - m_q \cdot (q - q_0) \tag{2.7}$$

Where, v^* is the reference voltage amplitude of the converter voltage, v_0 is the reference voltage, m_q is the droop coefficient, q is the measured reactive power and q_0 is the reference reactive power. The reactive power droop control structure can be implemented as a block diagram, as shown in Figure 2.4

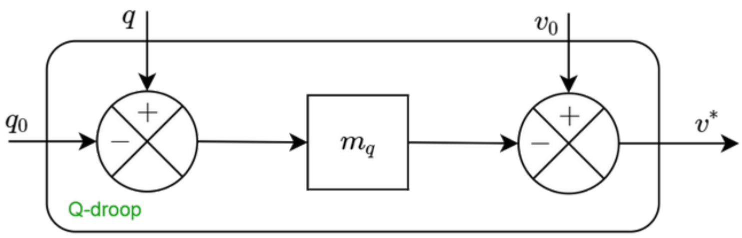

Figure 2.4: Reactive power droop control diagram

The first low level control method, voltage reference direct PWM, see Table 2.1, is the least complex. With this method, the voltage and rotor angle references from the droop and swing equation, respectively, are directly used as reference value for the pulse width modulation (PWM) signals to control the power modules in a power converter.

One issue encountered with this method is the difficulty in limiting the output current of the converter. No inherent control loops allow this operation. Thus, additional protection hardware will be required to limit the voltage and current. With the additional protection hardware, the interaction with the top level controller can be complicated. [20]

The second low level control method, voltage reference cascade control, see Table 2.1. With this control method, it is possible to limit both the voltage and current by saturation blocks in the control loop. Moreover, this control schema is well known from classical grid-following converters. The block diagram of this approach is displayed in Figure 2.5.

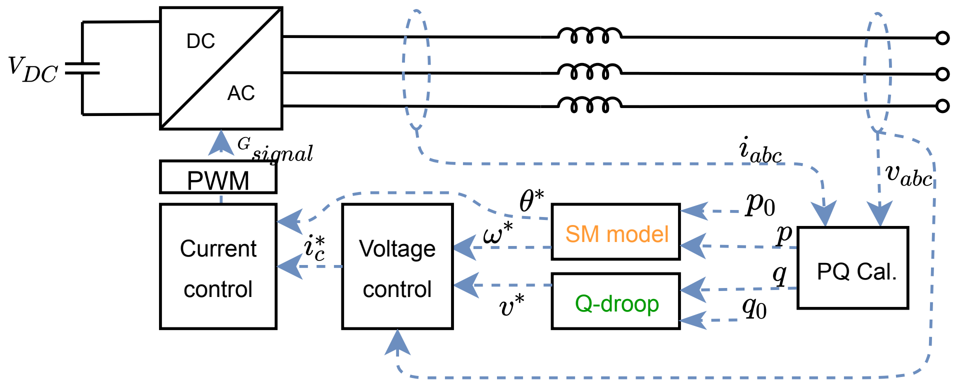

Figure 2.5: VSM control diagram with converter interface control.

The third low level control method, current reference hysteresis control, see Table 2.1. This control method is based on a detailed SG model, level of details can vary, where a current reference is calculated from the model which would be equal to the stator current generated by a real SG. A hysteresis controller is then applied to control the converter to inject the calculated current reference from the SM model. Saturation limits can easily be implemented on the current reference. However, utilising a hysteresis controller, which works with a fixed tolerance band will not have a constant switching frequency and will, therefore, generate a higher level of harmonics. [10][20]

2.4.2 Inertia emulation

The basic idea of Inertia emulation top level control is to detect power imbalance in a system by measuring the frequency variation or RoCoF. The is also achieved by utilising the swing equation, Equation (2.6), as for the VSM control. The swing equation is rearranged and expressed in Equation (2.8). [21]

$$\Delta P = P_0 - P = \frac{2H}{f_0}\frac{df}{dt} \tag{2.8}$$

As can be seen from Equation (2.8), based on the measured RoCoF (df/dt) the corresponding delta active power can be calculated, which will be required from the converter to support the system power balance. The additional active power will counteract the impact of, e.g. loss of an infeed. [22] [20] A block diagram of the Inertia emulation based top level control is displayed in Figure 2.6.

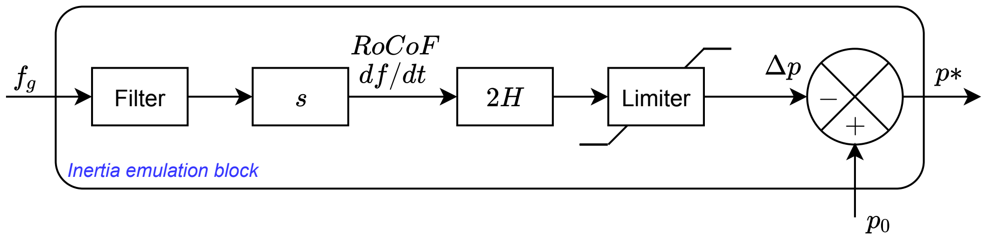

Figure 2.6: Block diagram of Inertia emulation model based on Equation (2.8).

The low level structure of the Inertia emulation is achieved from converting the power reference calculations to a current reference, based on the grid voltage measured by a PLL. A common block diagram of the Inertia emulation control, including the converter interface, is displayed in Figure 2.7. [21] [20] [22]

To measure an accurate RoCoF, which the power reference is calculated from, is particularly essential. This has so far been achieved with a fundamental PLL, which is also used in classical grid-following converters to synchronises the converter with the grid. Thus, the inertia emulation control method is dependent on a stable voltage reference from the PLL to operate correctly. The inertia emulation control will, therefore, not work in weak grid conditions or islanded operation [20]. Furthermore, to measure the frequency deviation a filter is typically required, which will slow down the detection time of a frequency deviation and thus impact the system inertia support. [21]

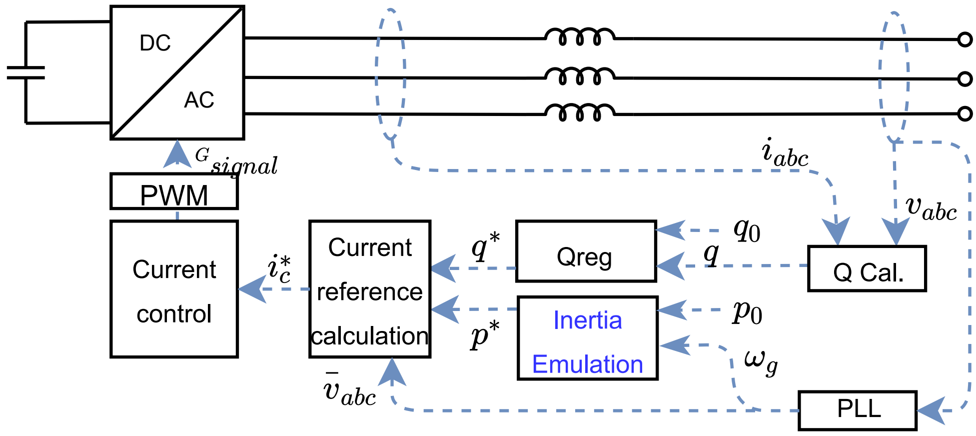

Figure 2.7: Inertia emulation control diagram with converter interface control.

2.4.3 Voltage injection concept

Voltage injection concept proposes to retrofit the conventional cascade voltage and current controller in the network bridge converter [23]. The concept is deduced for a full-scale converter WTG. The conventional full-scale converter control of a WTG is explained in Section 2.3.

The concept proposes to remove the integrator term in the conventional PI current controller and move the proportional term. The integrator term can be removed since upstreams integrator terms still exist in the voltage controller [23]. The proportional term is moved after the cross-coupling term and create an additional feed-forward term with a high pass filter. It can be visualised in Figure 2.8, where the conventional and new proposed scheme is shown. Thus, the conventional fast current controller characteristic is removed and left is only a static gain. It means only the slower voltage control loop is left with the up-stream integrator term, which will remove the error term.[23]

The new feed-forward term in the proposed q and-d axis controller is utilised to emulating a damping characteristic corresponding to a serial virtual resistor. Thus, the damping is achieved without any power losses. The high-pass filter is used to enable frequency-selective damping. Hence, the damping effect can be limited to transient (high frequency) currents only. [23]

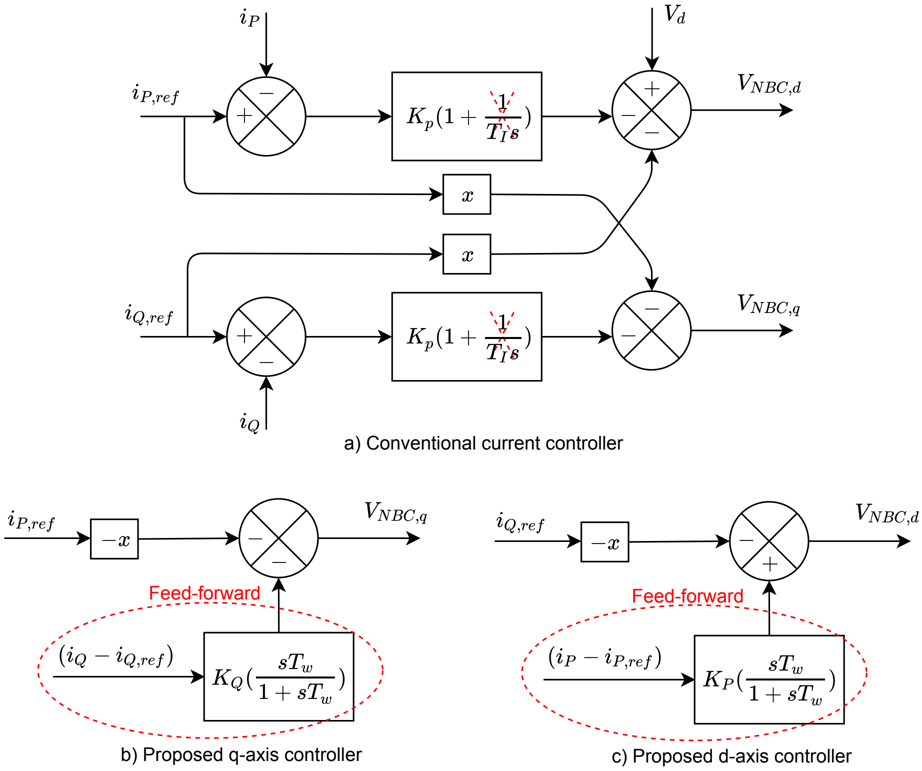

Figure 2.8: Proposed voltage injection concept based on [23]. a) shows conventional current controller in a WTG, b) shows the proposed q-axis current controller and c) shows the proposed d-axis current controller.

2.4.4 Droop controlled

The most dominant and common approach for microgrid grid-forming control is based on droop control. The active power and reactive power is controlled separately by two droops as shown in Equation (2.9) and Equation (2.10), respectively.

$$\omega^* = \omega_0 - m_p(p - p_0) \qquad \theta = \frac{1}{s}\omega^* \tag{2.9}$$

$$v^* = v_0 - m_q(q - q_0) \tag{2.10}$$

Two droop gains, m_p and m_q, are utilised to determine the required frequency and voltage from the converter, based on a deviation from the set-points p_0 and q_0, and the filtered measured active and reactive power, p and q. The instantaneous active and reactive power is calculated from the measured converter current and the calculated voltage reference from Equation (2.10). Since the power angle, δ, is derived from the droop controller, no PLL is required. The instantaneous power is averaged over one cycle by a boxcar filter, before the droop control. [18]

Since the output of the droop control is a voltage amplitude and phase angle, the droop control approach can utilise the same low level interface as the VSM method. A block diagram showing the control method of droop control is displayed in Figure 2.9.[18]

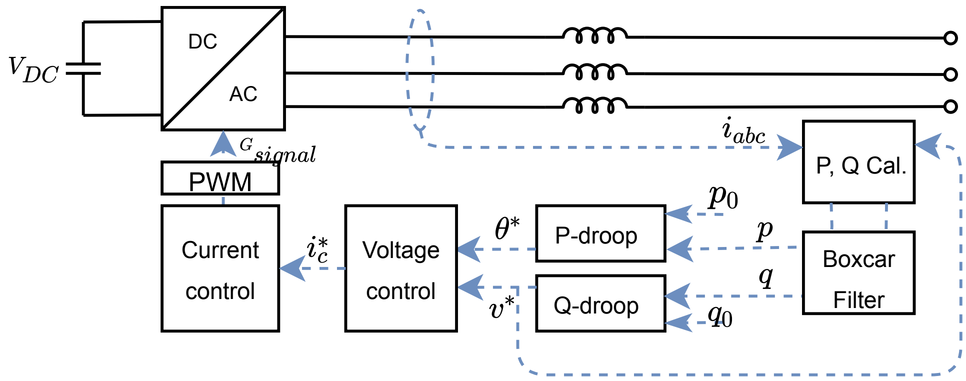

Figure 2.9: Diagram of droop control method with converter interface control.[20]

The two droop blocks Q-droop and P-droop in figure Figure 2.9 corresponds to Equation (2.9) and Equation (2.10), respectively. The droop controlled method enables converters to operate as a stable voltage source, connected to a grid via a filter impedance. Thus, the droop controlled method mitigates power quality issues. However, the droop controlled method does not mitigate against RoCoF following a disturbance, as no inherent inertia is emulated. However, the droop control method will still help to reduce the frequency nadir.[20]

Summary of GFC methods

From the analysis of the different GFC control concepts, it can be concluded that the inertia emulation control method is not compliant with ENTSO-E's definition of a grid-forming unit since it will not represent a voltage source behind an impedance.

Furthermore, it can be concluded that control approaches exist which does not exactly mirror the control of an SG. However, ENTSO-E's working group recommend defining the characteristics of a GFC similar to an SG, even though the control scheme might not be directly comparable. Thus, the GFC characteristic should be defined based on inertia constant and a damping factor. It will make it more agreeable for TSOs to understand the capabilities of GFCs.

2.5 Technical considerations of applying GFC control to WTGs

Wind turbines have been designed to operate as grid-following units, as explained in Section 2.3. Thus, applying GFC to WTGs will create new challenges, which need to be considered. These challenges will be described in this section.

The challenges arising from applying GFC to WTGs can be categorised into three main categories, which are operational boundaries, parameterisation, and WTG physical limit. Each category will be explained below. [2]

Operational boundaries:
The operational boundaries are describing the conditions for the power system, where the GFC is expected to retain its grid-forming characteristics. The operational boundaries can be defined by the TSOs and will consider frequency range, RoCoF, voltage imbalance, fault current contribution and phase step. Defining these operational boundaries will describe the required operation conditions for GFCs. [2]

Parameterisation:
The parameterisation is describing the supporting characteristics of a GFC. The parameterisation is desirable to be defined in terms of the already recognised parameters used by the power system industry, as explained in Section 2.4. These parameters are the inertia constant, H, and damping ratio. An additional feature to consider is a frequency-droop controller. However, a frequency-droop controller is not an inherent grid-forming characteristic, but rather an add-on feature known from conventional SGs. [2]

WTG limitation:
Implementing grid-forming characteristics to a WTG will present some limitations. One limitation to consider, is the converter hardware, as the semiconductor modules, which are utilised in the power converter have a maximum current capability. Thus, to prevent damage of the semiconductor modules, the peak current must not violate the converter capability. [2]

Another limitation to consider, is the energy which can be extracted from a WTG owing to a system disturbance. Considering a generic full-scale converter WTG, as presented in Section 2.3. A WTG's generator is controlled by the generator bridge converter (GBC), which is connected to the network bridge converter (NBC). If a frequency disturbance occurs, an increase or decrease in power will be supported by the NBC, which is per definition of a grid-forming unit. Consequently, this will provoke the GBC to feed more power to the DC link capacitor to maintain the DC link voltage. It inherently means a WTG's generator will be coupled to system frequency disturbances when operating in grid-forming mode. [3]

As WTGs are restricted by the wind conditions, the operating condition of a WTG during a frequency disturbance can create additional complications. If a WTG is generating a low power, owing to low wind speed, and is subjected to a negative RoCoF, the contribution of energy from the WTG will be close to zero since limited energy is stored in the WTG rotor. Oppositely, if a WTG is subjected to a positive RoCoF during low wind speed conditions (low power), the incoming energy can not be accumulated by the rotor, since the rotor speed is already close to the cut-out speed. Thus, the DC capacitor is the only source to accumulate excess energy, which will lead the DC bus voltage to rise undesirably.

Thus, it is evident that additional energy is required, for WTGs to operate in grid-forming mode to support the entire frequency envelope as SGs, during all operating conditions. [13] The additional energy can be obtained from a reduction in the steady-state output setpoint (Curtailment of WTGs), adding storage (battery or super capacitor) or extracting stored rotor energy form the blades of WTGs. Alternatively, a combination of all three can be used to present a solution to gain a higher energy buffer. [13][19]

Consideration of GFC characteristics based on system disturbance:
The response of a GFC based on a system disturbance can be split into a disturbance in energy and a peak current demand. The amount of energy required from a GFC to support a system disturbance depends on the inertia constant, H, and the change in system frequency. The energy demand can be estimated from Equation (2.11). [3]

$$\Delta E = H \cdot S_{base} \frac{f_{pre}^2 - f_{nadir}^2}{f_{pre}^2} \tag{2.11}$$

Where, S_{base} is the base power of a given unit and f_{pre} is the pre-event frequency, and f_{nadir} is the frequency nadir during the frequency event. If a WTG operating in grid-forming mode is expected to support the same frequency envelope as conventional SGs, the frequency envelope will range from 47.5 Hz to 51.5 Hz, based on ENTSO-E continental grid code [24]. Even though a frequency change of 4 Hz is most unlikely. However, it is essential to make sure that WTGs running in GF mode will not run out of energy before the frequency reaches below 47.5 Hz. [3]

The peak current demand expected from a WTG operating in a grid-forming mode, based on a system disturbance, can be calculated from Equation (2.12). The peak power demand depends on the RoCoF, (df/dt), and the inertia constant, H. The amplitude of the peak power demand will yield the peak current demand. [3]

$$\Delta P = \frac{2H \cdot S_{base}}{f_0} \cdot \frac{df}{dt} \tag{2.12}$$

Where S_{base} is the base power, and f_0 is the nominal system frequency. The damping characteristic also needs to be considered when determining the maximum power demand by a grid-forming unit. The damping characteristic influence the rate at which the new power reference is reached. It is desirable to have robust damping to avoid interaction with external power system controllers. However, depending on the tuning of the damping, overshoot in the power response can occur, which will lead to higher peak demand. Hence, the inertia constant, together with the damping characteristic, will have a significant impact on the required converter rating. [13]

Consideration of GFC design based on fault event:
WTGs converters rating is highly depending on the short circuit current contribution. In case, a close-in fault occurs, and a WTG is operating in grid-forming mode, it can lead to a substantial current demand. If such situations are not avoided, or the converter is capable of handling the current, it can lead to the WTG will trip. [13][19][25]

Short circuit current from SGs is mostly limited from the inherent impedance within SGs and is mostly dominated by thermal constraints. During a system fault, SGs can typically deliver a substantial and instantaneous fault current between 5 to 8 pu [26]. Contrary, the short circuit current from WTGs is limited from the rating of the semiconductor modules in the converter. Thus, a more strict limit will exist for WTGs. As the power system traditionally has been comprised of SGs and the inherent high fault current, power system protection is design to rely on this behaviour as well. Furthermore, a high fault current will also benefit from restricting the voltage decline throughout the power system during a fault event. Thus, the fault current contribution from grid-forming units is an essential property to consider. [26]

National Grid has initialised an investigation of grid code requirements for fast fault current injection, where one of the investigated solutions are grid-forming control of converter based power sources. From this investigation, a fault current magnitude of 1.5 pu is proposed to maintain a sufficient fault current level. [26]

Based on National Grid's proposed fault current level of 1.5 pu WTG converters will need to be scaled up as they are typically rated to 1.1 to 1.2 pu current. Furthermore, if a current limit of 1.5 pu is considered, the peak current demand during a frequency disturbance should then also be limited to this value. [19]

Consideration of specifying GFC characteristics:
As mentioned, GFC support characteristics can be split up into three categories. Depending on how the categories are considered, the GFC requirements will be different.

If the operational boundaries and parameterisation are specified by, e.g. a TSO, the required hardware for converter and energy storage should be designed accordingly. Hence, depending on the range of the operational boundaries and selection of parameterisation, the cost can be high.[2]

The second approach considers the hardware as being the limiting factor. Thus, the parameterisation and operational boundaries will then be specified with respect to the hardware limits. It will have a lower cost, but also lower system support.[2]

2.6 Summary

In this chapter, it was presented how power system stability can be classified together with the definition of a stable and unstable system. It was then elaborated how synchronous generators act to system disturbances and how this can be described by the swing equation. The general converter control of a full-scale converter wind turbine was then presented. It was elaborated how WTGs uses a PLL to synchronise the converter to the grid and that WTGs are operated as grid-following units.

It was then explained how VSM, Voltage injection concept and Droop controlled control methods can be utilised, to obtain grid-forming behaviours for converter based power units. Based on the state of the art analysis, it is decided to use the fundamental from the VSM control concept to develop an aggregated grid-forming model of a wind farm. This method is used, as it is possible to mirror the desired dynamics of an SG and as the grid-forming model will be conducted in the RMS domain with phasor representation.

Lastly, different practical limitations when applying grid-forming control to WTGs were described. It was explained, how the inertia constant, frequency envelope, WTG operating condition, fault current contribution, and damping characteristic is vital features to consider if GFC control os applied to WTGs.

Chapter 3

Development of a grid-forming WTG model

In this chapter, it will be explained how a GFC model of a WTG can be set-up and implemented into the simulation software DIgSILENT PowerFactory.

The grid-forming model is implemented as a dynamic RMS model with the utilisation of PowerFactory's dynamic simulation language (DSL). It means the model is based on dynamic phasor representation in RMS quantities. Thus, in steady-state operation, the AC vector quantities will be constant. RMS models present some limitations as they are typically simplified and utilising only positive sequence components. Thus, only the fundamental components of voltages and currents are considered, which means harmonics will not be treated. An alternative simulation approach to RMS simulations is the electromagnetic transients (EMT) which consider the instantaneous values of voltages and currents and therefore capture the full detail and interactions of models. However, EMT simulation speed is significantly slower compared to RMS simulations, which is why RMS simulations are typically used on grid-wide systems. RMS simulations are, therefore, essential to TSO's as RMS studies are one of the primary methods used to do day to day assessment of the power systems together with dynamic analysis in planning. [2][27][19]

Wind farms are typically represented as aggregated models in power system studies conducted by, e.g. TSOs. It is done to reduce simulation time. It means the individual WTGs and the collector network of a wind farm is simplified to a single power unit with an equivalent impedance to represent the wind farm. Aggregated models can be utilised for RMS simulations without losing significant accuracy [28]. The GF model described in this section will, therefore, also represent an aggregated wind farm. [28]

3.1 GF model implementation

As explained in Section 2.4, a variety of grid forming converter control concepts exist. The GF model implemented in this chapter is implemented. With the utilisation of the VSM control concept as introduced in Section 2.4. This control concept is used as the GF model is implemented to represent an aggregated wind farm.

A control diagram of the GF model implemented into PowerFactory is displayed in Figure 3.1. The control diagram illustrates the connections of the different DSL blocks created in PowerFactory.

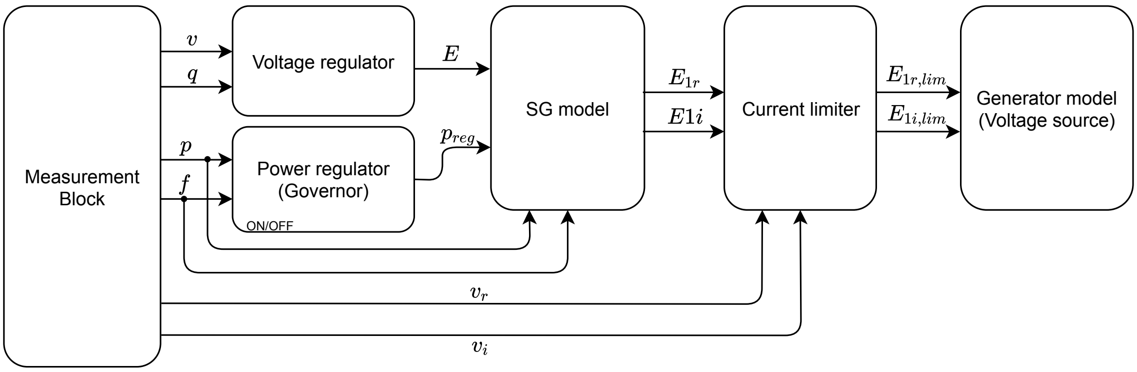

Figure 3.1: Illustration of control block of the GF model implemented into PowerFactory. v is the measured terminal voltage, q is the measured reactive power, p is the measured active power, f is the measured grid frequency, vr and vi is the real and imaginary voltage component of v, E is the positive sequence converter voltage, $E1r$ and $E1i$ is the real and imaginary voltage component of E and $E1r_{lim}$ and $E1i_{lim}$ is the limited voltage reference sent to the voltage source.

As it can be seen from Figure 3.1, the GF model consists of a voltage regulator, a power regulator, an SG model, a current limiter and a generator model which is a controllable voltage source. The measurement signals to the GF model is collected in the measurement block. Each block from Figure 3.1 will be described in the sections below, starting with the generator model as this is the source element representing the GF source.

3.1.1 Generator model

The static generator model in PowerFactory is typically used to represent non-rotating generators, such as photovoltaic generators, storage devices and full-scale converter wind turbines [27]. Thus, the static generator model is utilised for the GF model. The static generator model is controlled as a voltage source. The layout of the static generator model is displayed in Figure 3.2.

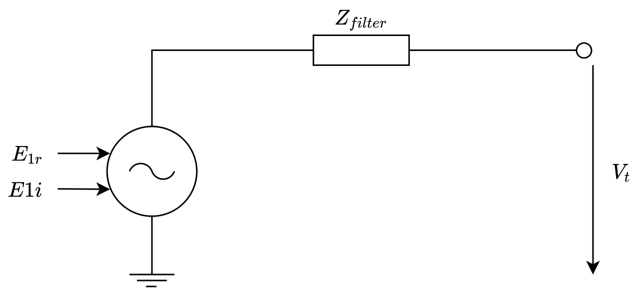

Figure 3.2: Schematic of the voltage source model of a static generator in PowerFactory

The static generator model in Figure 3.2 requires two input signals to control the voltage source, which are the real and imaginary positive sequence voltages, E_{1r} and E_{1i}. The impedance Z_{filter} represents the aggregated equivalent wind farm impedance, and V_t is the terminal voltage of the aggregated wind farm.

3.1.2 Voltage regulator

A voltage regulator is implemented based on a voltage droop controller. It means the reactive power contribution form the GF model depends on the deviation in system voltage from the reference voltage value. It can be described mathematically by Equation (3.1).

$$v_{err} = V_{ref} - q \cdot m_q - v \tag{3.1}$$

Where, V_{ref} is the reference voltage, q is the measured reactive power, m_q is the droop gain and v is the measured terminal voltage. As it can be seen in Figure 3.3, a PI controller is implemented to processes the voltage error V_{err} from the voltage droop controller. The output signal of the PI controller is passed through a low-pass filter. The low-pass filter is used to ensure that the GF model will represent a slow-moving voltage source.

The voltage droop controller has a fixed voltage reference V_{ref} as input, which is the tar-

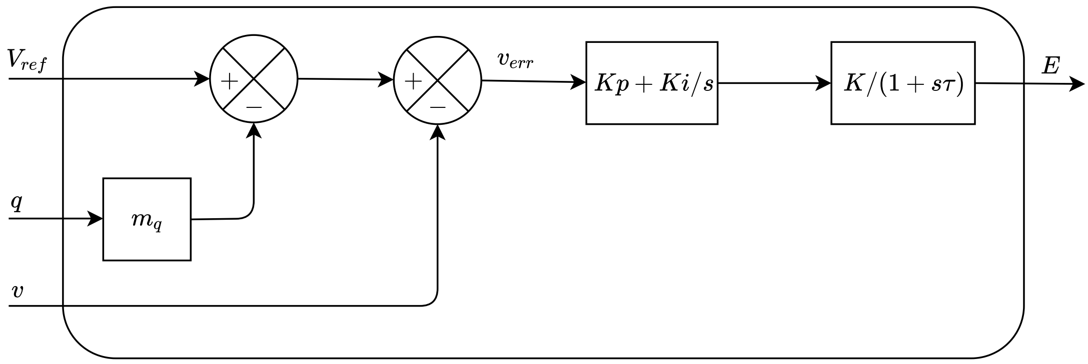

Figure 3.3: Block diagram of voltage regulator implemented in PowerFactory

get voltage for a specific bus terminal in the system. In this case, the reference terminal voltage is the terminal of the static generator, V_t. If the measured voltage at the reference bus terminal deviates from the voltage reference, the reactive power support from the GF model will change proportionally. The relationship between voltage and reactive power is displayed in Figure 3.4. As can be seen from Figure 3.4, if the measured voltage

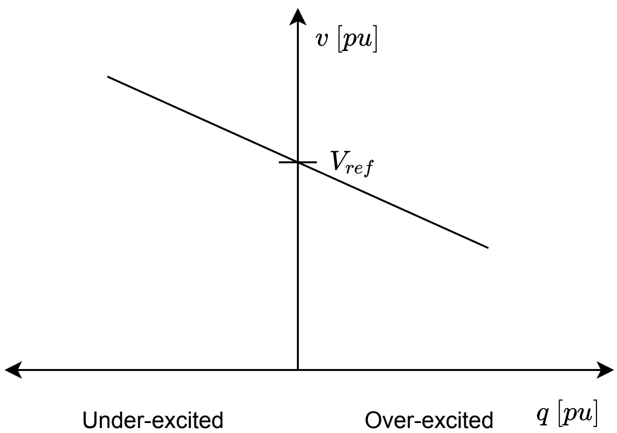

Figure 3.4: Relationship between voltage and reactive power based on droop gain m_q.

is below the reference value, the voltage regulator will contribute over-excited and increase the reactive power output. The droop gain m_q dictate the slope in Figure 3.4 and the relationship between the measured voltage and reactive power. Thus, by adjusting the value of m_q, the voltage droop controller will become more or less aggressive. For instance, with an m_q value of 1% and a voltage deviation of 0.01 pu, the reactive power contribution from the generator will be 100% of the nominal apparent power. The droop value of m_q is often selected to be 4-5% [7].

3.1.3 Power regulator

A power regulator block is added to gain a similar behaviour as the power-speed controller of a conventional SG. The power-speed controller in an SG, regulates the valve position in order to increase or decrease the mechanical output power of the rotor, which is done in relation to the measured system frequency [14]. The same principle can be enabled by utilising a frequency droop controller in the GF model. The frequency droop controller is expressed in Equation (3.2).

$$(f_{ref} - f)m_p + (p_{set} - p_{reg}) = 0, \qquad m_p = \frac{1}{\rho} \tag{3.2}$$

Where f_{ref} and f are the reference frequency and the measured system frequency, respectively. ρ is the droop coefficient in percentage of the GF models power rating and m_p is the effective gain. p_{set} is the operating power set-point of the GF model. If the system frequency deviates from the reference frequency the active power reference p_{reg} will change accordingly, as can be seen from Equation (3.2). From Equation (3.2) the control block diagram for the power regulator can be obtained as in Figure 3.5. In steady-state

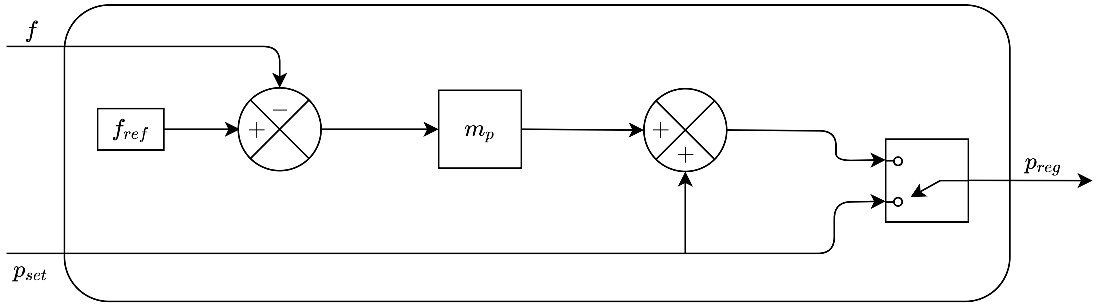

Figure 3.5: Block diagram of power regulator implemented in PowerFactory.

conditions the output power, p_{reg}, will be equal to the operating power set-point, p_{set}. A selector block is implemented to the control block diagram shown in Figure 3.5, to enable or disable the frequency droop controller, when the model is offline. This is done, as the frequency droop controller is not an inherent dynamic property of a grid-forming unit, but rather an add-on feature to mirror the behaviour of conventional SG. Hence, the frequency droop controller can be bypassed and the power regulator will operate with a fixed power reference, which will represent the power set-point of a WTG. [2]

3.1.4 SG model

The SG model block is implemented to gain the inherent inertia and damping response of a real SM. It is achieved by emulating the rotor dynamic of a real SM. The implementation in PowerFactory is based on the VSM theory presented in Section 2.4. The implemented block diagram of the SG model in PowerFactory is displayed in Figure 3.6

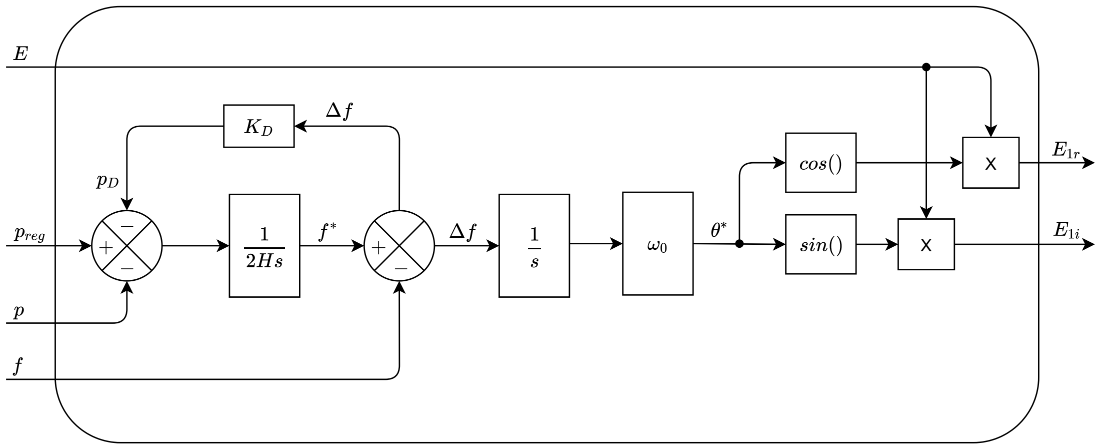

Figure 3.6: Block diagram of SG model implemented in PowerFactory.

If an error exists between the power reference p_{reg} and the measured output power of the GF model, p, the error is passed through the integrator term ($1/2Hs$), where, H, is an equivalent inertia constant. The output signal of the integrator term is the estimated system frequency, f^*. Thus, if the connected power system is in equilibrium and the power error is zero the estimated frequency output will be equal to the system frequency (e.g. 1 pu). The system frequency, f, is measured with a PLL block from PowerFactory's library.

Subtracting the measured system frequency, f, from the estimated system frequency, f^*, will yield frequency deviations. A feedback damping term is added to the summing junction of the power if a frequency deviation exists. In steady-state, the damping term will be zero. If a frequency deviation exists, the angle θ^* will rotate the real and imaginary AC voltage vectors components. Hence, the real and imaginary AC voltage vector components E_{1r} and E_{1i} are rotated depending on the system condition. If the connected power system is in equilibrium, the angle θ^* will be constant to deliver the desired power reference p_{reg}, hence, θ^* is equivalent to the rotor angle of an SM. The rotor angle output of the block diagram in Figure 3.6 can be described by Equation (3.3).

$$\theta^* = \frac{\omega_0}{s}\left(\frac{1}{2Hs}(p_{reg} - p - K_D\Delta f)\right) \tag{3.3}$$

If small signal perturbations are applied to the SG model and Equation (3.3) is linearised, the describing equation of the rotor angle can be derived as in Equation (3.4).

$$\Delta\theta^* = \frac{\omega_0}{s}\left(\frac{1}{2Hs}\left(\Delta p_{reg} - K_S\Delta\theta^* - \frac{\Delta\theta^*}{\omega_0}sK_D\right)\right) \tag{3.4}$$

The electrical power output, p, can be expressed as the linearised power about an initial operating condition ($\theta^* = \theta_0^*$), as shown in Equation (3.5).

$$\Delta p = \frac{\partial p}{\partial\theta^*}\Delta\theta^* = \frac{EV}{X_{tot}}cos(\theta_0^*)\Delta\theta^* = K_s\Delta\theta^* \tag{3.5}$$

Where, E is the converter voltage and V the external system voltage and X_{tot} is the total reactance in between the two bus voltages. However, it should be noted that Equation (3.5) is only applicable for steady-state phasor values The linearised power in Equation (3.5) is denoted, K_s, and is known as the synchronising power coefficient, which is the electrical power required to reach synchronous operation owing to a system disturbance. From Equation (3.4), the transfer function for the rotor angle can be derived as in Equation (3.6).

$$\frac{\Delta\theta^*}{\Delta p_{reg}} = \frac{\frac{\omega_0}{2H}}{s^2 + \frac{K_D}{2H}s + \frac{K_s}{2H}\omega_0} \tag{3.6}$$

The characteristic equation of Equation (3.6) is shown in Equation (3.7) where the general form is shown in Equation (3.8).

$$s^2 + \frac{K_D}{2H}s + \frac{K_s}{2H}\omega_0 = 0 \tag{3.7}$$

$$s^2 + 2\zeta\omega_n s + \omega_n^2 = 0 \tag{3.8}$$

Where, ω_n is the natural frequency and ζ is the damping ratio. Comparing the two characteristic equations, it can be found that the damping ratio of the SG model, can be estimated from Equation (3.9).

$$\zeta = \frac{1}{2}\frac{K_D}{\sqrt{K_s 2H\omega_0}} \tag{3.9}$$

3.1.5 Current limiter

A current limiter block is added to the GF model to constraint the output current of the GF model. It is done as real converter based power sources will have a limited current carrying capability, as explained in Section 2.5.

The calculated voltage vectors E_{1r} and E_{1i} from the SG model block are passed through the current limiter block before processed in the generator block.

The current limiter block is based on a maximum allowed voltage drop over the filter impedance. If the notations from Figure 3.2 is considered, the voltage drop over the filter is given in Equation (3.10)

$$V_{filter} = E - V_t \tag{3.10}$$

where the maximum allowed voltage drop over the filter is given by the maximum allowed converter current, as shown in Equation (3.11).

$$V_{filter,max} = I_{max} \cdot Z_{filter} \tag{3.11}$$

Hence, V_{filter} needs to be limited to $V_{filter,max}$. This current limiting algorithm is implemented in the GF model in PowerFactory accordingly to Figure 3.7. Note, Figure 3.7 is only displaying the current limiting algorithm for the real voltage component. It is done for simplicity. The same algorithm is applied for the imaginary component of the voltage. The filter voltage $V_{r,filter}$ is normalised based on the calculated filter voltage

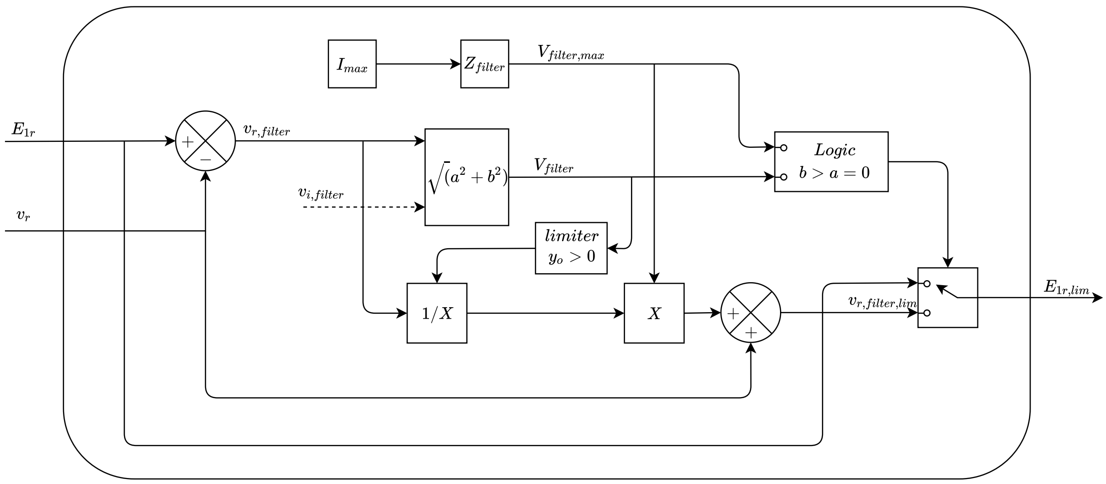

Figure 3.7: Current limiting control diagram, for the real voltage component, implemented in the GF model.

magnitude V_{filter}, which is limited to above zero for numerical reason. In normal operating condition, where the current limit is not violated, the two switches before the output will bypass the current limiting block and $E_{1r,lim}$ will be equal to E_{1r}. However, if the voltage drop over the filter impedance exceeds the maximum allowed voltage, the two switches before the output will be enabled by the logic block and the output will become $V_{r,filter,lim}$. The voltage reference sent to the static generator will then be limited to ensure the maximum current I_{max} is not violated. [25]

3.2 Evaluation of GF model

This section is written to evaluate the dynamic response of the GF model presented in Section 3.1. A test system is implemented into PowerFactory in order to evaluate the response from the GF model. The test system is displayed in Figure 3.8. The test system

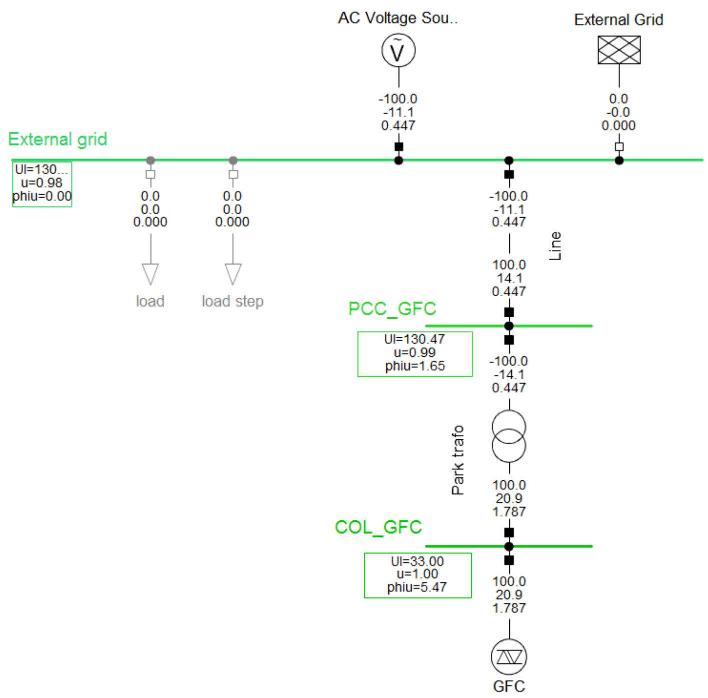

Figure 3.8: Screenshot of test system setup in PowerFactory to evaluate the GF model presented in Section 3.1

consists of a GF model representing an aggregated wind farm, a park transformer to step up the voltage, a transmission line to connect the GF model to an external system. The ratings and parameters of the different elements are summarised in Table 3.1. The per-unit values of the listed elements in Table 3.1 are based on a base power of 175 MVA, except the park transformer, which is based on its power rating.

Table 3.1: Ratings of the different elements of the test system shown in Figure 3.8

Elements	V [kV]	S [MVA]	X [pu]	R [pu]
GFC	33	175	0.1	-
Park Trafo	33/132	190	0.125	0.004
Line	132	-	0.049	0.005
External grid	132	Sk''_{max} = 1000	X/R = 10	

The parameter Sk''_{max} listed in Table 3.1 is the short circuit power of the external system where an X/R ratio of 10 is applied. The short circuit ratio (SCR) of the test system can be calculated from Equation (3.12),

$$SCR = \frac{Sk''_{max}}{P_{rated}} \tag{3.12}$$

which yields an SCR of approximately 6. An SCR higher than 5 is representing a strong grid connection [15]. An ideal AC voltage source is also added to the external grid terminal. The AC voltage source is utilised to change the external systems voltage amplitude and system frequency.

The different control blocks in the GF model is evaluated based on the following test cases:

- Voltage reference step
- External voltage ramp event
- Frequency change
- Pseudo RoCoF
- Load step
- External fault event

The results from the different test cases of the GF model are presented in the subsequent sections.

3.2.1 Evaluation of voltage regulator

The first dynamic test of the GF model will evaluate the voltage regulator described in Section 3.1.2. A voltage step of 5% is applied to the voltage reference signal V_{ref} in Figure 3.3. The response of the voltage regulator is displayed in Figure 3.9.

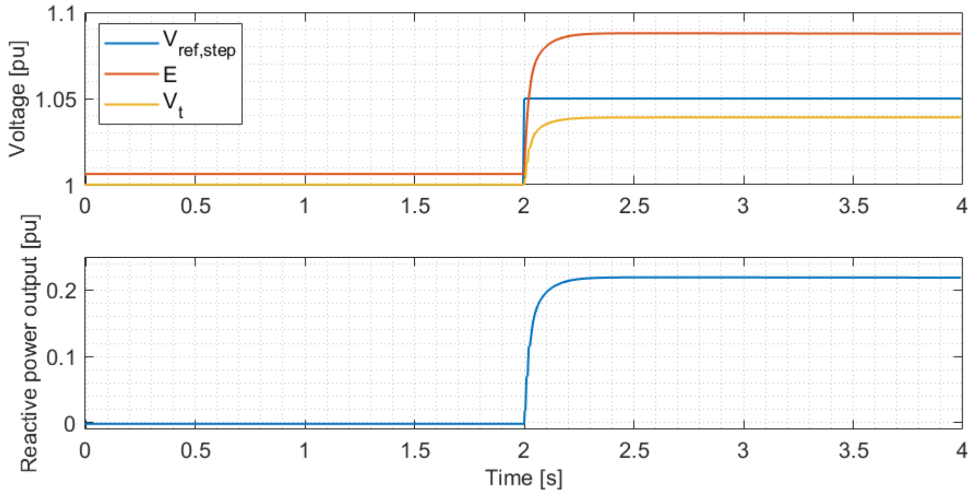

Figure 3.9: Evaluation of a 5% voltage step applied to the voltage reference in the voltage regulator in the GF model.

As can be seen in Figure 3.9, applying a step to the voltage reference of the voltage regulator it will increase the voltage at the converter terminal, V_t. It is achieved by increasing the internal converter voltage E. The converter terminal voltage, V_t, is measured at bus *COL_GFC* in Figure 3.8. A droop gain of 5% is applied to the voltage regulator. From Figure 3.9, it can be seen, the voltage regulator response due to a voltage step is fast with a rise time of 0.089 s and with no overshoot.

The second dynamic test of the GF model will evaluate the reactive power response of the voltage regulator. It is realised by applying a voltage ramp to the external system voltage. The external system voltage is ramped up by 5% from 1 pu to 1.05 pu. Figure 3.10 displays the dynamic response of the GF model.

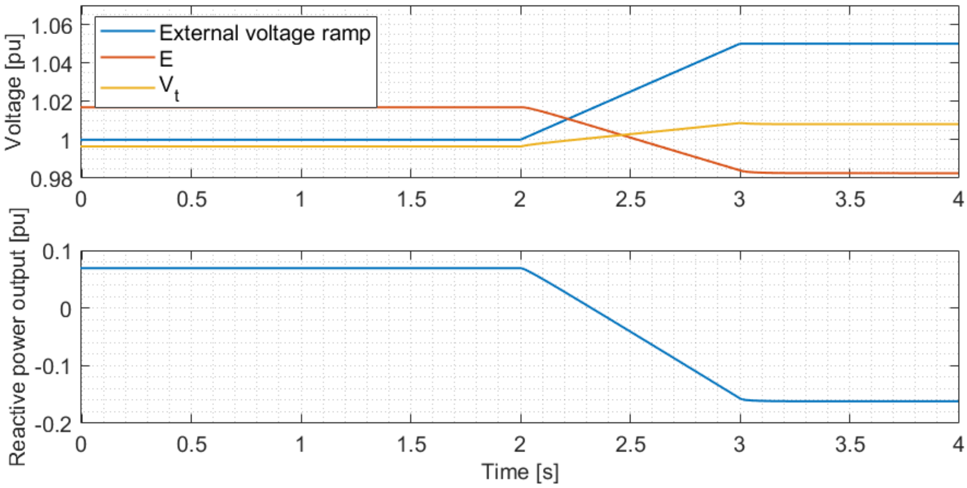

Figure 3.10: Response of the voltage regulator in the GF model due to an external voltage ramp increase of 5%.

From Figure 3.10, it can be seen that the pre-event reactive power output of the GF model is positive. It implies that the GF model is operating over-excited and generating reactive power. It is the case when the converter terminal voltage V_t is below the converter internal voltage, E. Hence, the GF model is assisting in maintaining the system voltage. The post-event reactive power output of the GF model is then changed to be negative. Thus, the GF model is now operating under-excited and absorbing reactive power to support the system voltage. The amount of reactive power absorbed by the GF model is determined from the droop gain m_q, which is selected to be 5%. The converter terminal voltage increases with 0.008 pu, due to the voltage increase of the AC voltage source. It will yield a reactive power contribution of 0.16 pu. The reactive power contribution is per explanation of Figure 3.4 and can be examined visually from the dynamic response displayed in Figure 3.10.

3.2.2 Evaluation of power regulator

The third dynamic test of the GF model is evaluating the active power regulator control block, where the frequency-droop controller is enabled. The system frequency is alternated with the ideal AC voltage source to three different set-points of 0.98, 1 and 1.01 pu where different ramp rates are applied. The change of the active power set-point from the power regulator is determined by the droop gain, ρ, as shown in Equation (3.2). A droop gain of 4-5% is typically used for SGs [29][14]. Thus, a droop gain of 5% is applied to the GF model to test the response. The active power set-point of the GF model is 0.57 pu (100 MW). The test result is displayed in Figure 3.11. As it can be seen in

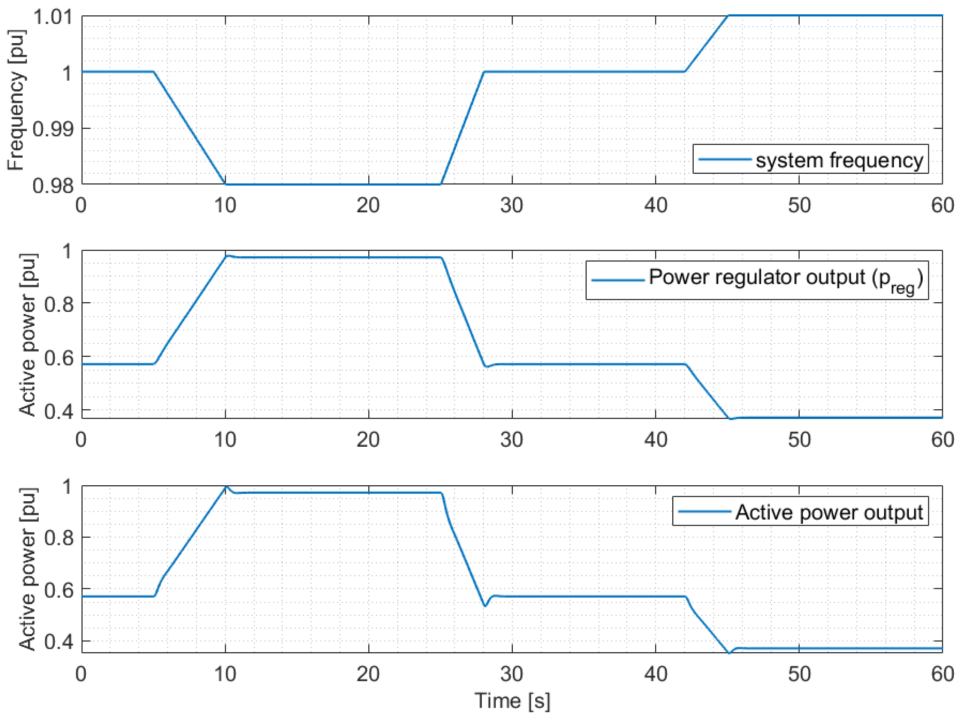

Figure 3.11: Evaluation of the power regulator in the GF model owing to a pseudo frequency change of 0.02 pu.

Figure 3.11, the active power set-point p_{reg} of the power regulator block will alter as the system frequency deviates from the reference frequency of 1 pu. The new p_{reg} set-point will provoke the active power output of the GF model to change accordingly, to the new steady-state value. Based on a droop gain of 5%, it implies that a frequency change of 0.02 pu (1 Hz) will increase the active power set-point by 0.4 pu (70 MW), which can also be examined visually in Figure 3.11. An increase in the active power of 0.4 pu owing to a 0.02 pu frequency decrease is substantial and will imply that the GF model representing a generic wind farm is required to run curtailed or have additional dedicated storage to meet this active power increase. Hence, if the frequency droop controller is enabled in the GF model the droop gain, is an essential parameter to consider. The frequency droop controller is disabled for the rest of the evaluation of the GF model.

3.2.3 Evaluation of SG model

Three different pseudo RoCoFs are applied to external AC system source to evaluate the respond of the GF model to frequency deviations. An inertia constant of 4 is selected for the GF model together with an active power set-point of 0.57 pu (100 MW). The result of applying the three pseudo-RoCoFs is displayed in Figure 3.12. Notice, the droop controller in the power regulator of the GF model is disabled. From Figure 3.12, it can

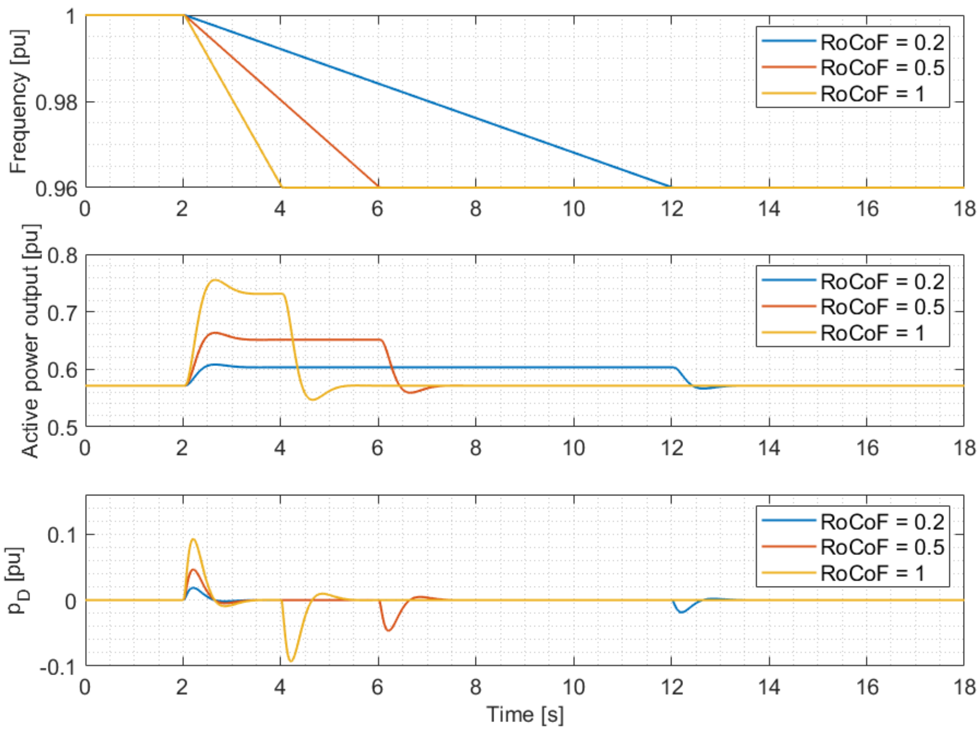

Figure 3.12: Evaluation of the GF model owing to three pseudo RoCoF events. The inertia constant of the GF model is 4 and the damping factor is selected to respond overdamped.

be seen how the active power response depends on the RoCoF. The higher the RoCoF, the higher the active power response, which is similar for the damping power p_D, as shown in Figure 3.12. The active power response has a small overshoot. It means the damping ratio is slightly underdamped. The increase of the active power response of the GF model owing to the applied RoCoF can be verified from Equation (3.13).

$$\Delta P = \frac{2HS_{base}}{f_0} \cdot \frac{df}{dt} \tag{3.13}$$

Thus, considering, e.g. the RoCoF of 0.5 Hz/s, where H is 4, f_0 is 50 Hz, and S_{base} is 175 MVA, an active power increase of 14 MW (0.08 pu) is expected. It can be verified visually by examining Figure 3.12.

Damping factor response

The response of the damping factor in the GF model is evaluated in Figure 3.13. A frequency deviation equal to a RoCoF of 0.5 is applied to the external system source. As the damping factor in the GF model can be freely selected, it is possible to obtain different damping response. Three different damping ratios, ζ, of 0.1, 1 and 3 are evaluated in Figure 3.13. These three damping ratios yields an underdamped, critically damped and overdamped response, respectively. The damping factor, K_D, of the GF model is calculated from Equation (3.9) based on the three damping ratios. The equivalent system impedance in Equation (3.9) is calculated from Table 3.1. Based on the three damping ratios, the damping factor K_D is found to be 20, 195 and 585, respectively.

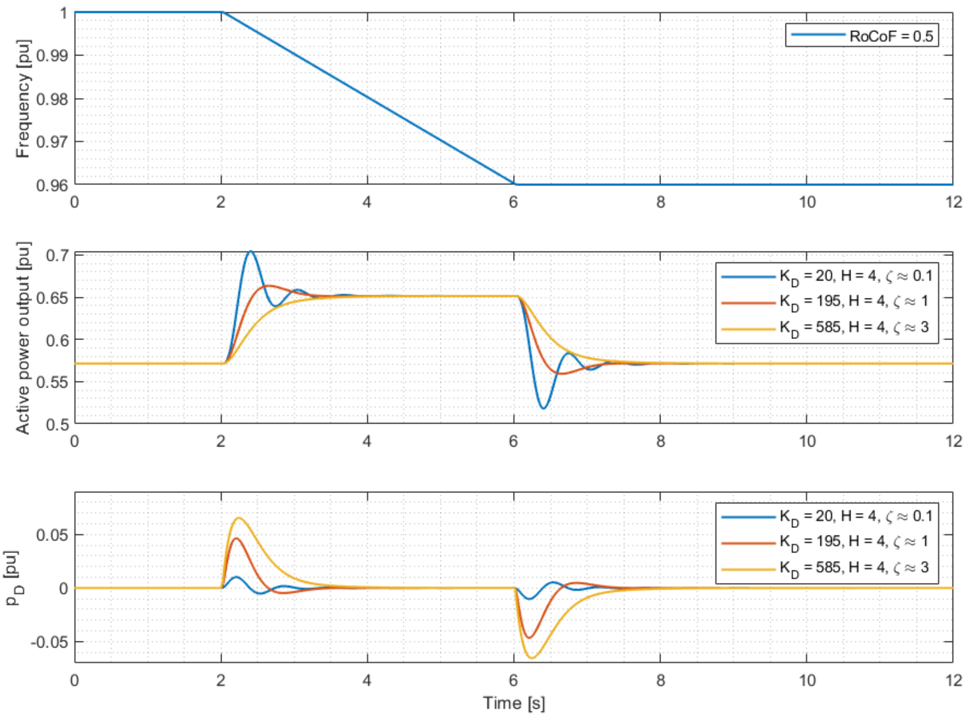

Figure 3.13: Evaluation of the GF model owing to a pseudo RoCoF event of 0.2, where three different damping factors are applied.

The damping response from the calculated damping factor can be examined visually in Figure 3.13. The damping ratio in Figure 3.13 deviates slightly from the desired damping response, as the response of the critically damped power has a small overshoot indicating the response is actually slightly underdamped. It can also be observed from the feedback damping power, p_D. Furthermore, it can be seen that the feedback damping power, p_D, is zero during steady state conditions.

It can also be seen from Figure 3.13, that the less damped response ($K_D = 20$) respond faster than the others but generates overshoots. However, it is often desirable in terms of a power system that the injected power response owing to a system disturbance is damped. It will minimise the risk of the GF model to interact unintentionally with external system controllers. Hence, a trade-off exists in terms of selecting the desired damping response of the active power output.[2]

Inertia response

The response of the inertia constant in the GF model is evaluated in Figure 3.14. A RoCoF of 0.5 is applied to the external system source. The GF model is selected to have a damping factor, K_D, of 195, where three different inertia constants of 2, 4 and 8 are applied.

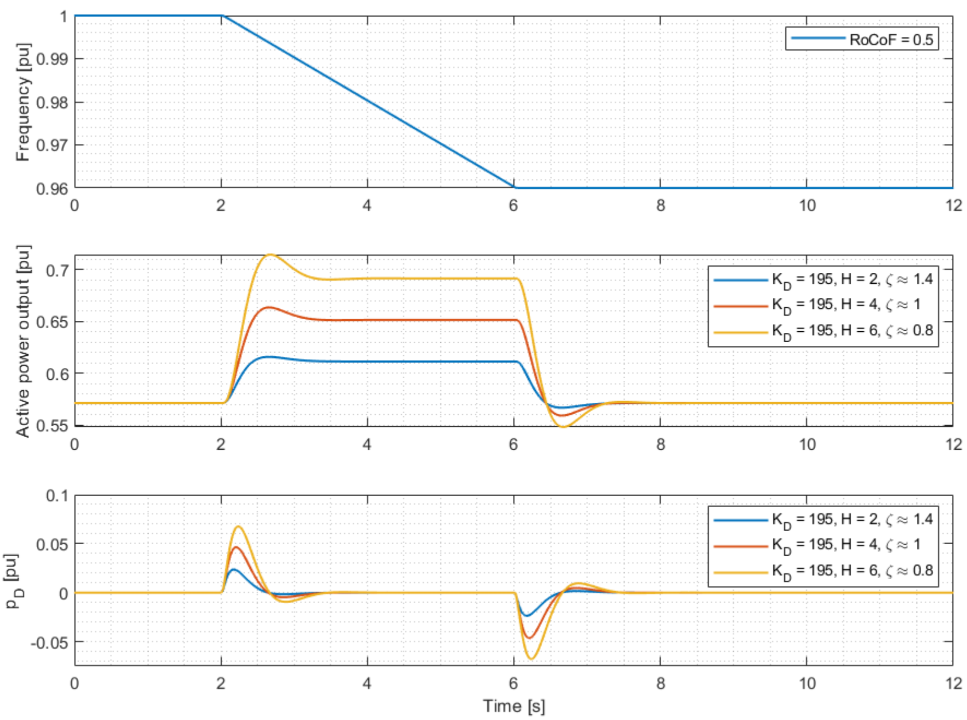

Figure 3.14: Evaluation of the GF model owing to a pseudo RoCoF event of 0.2, where three different inertia constants are applied.

From Figure 3.14, it can be concluded that the active power amplitude depends on the selected inertia constant, which is also per definition of Equation (3.13). E.g. consider, H equal to 6, the active power increase will be 0.12 pu (21 MW). It can be examined in Figure 3.14 as well. Furthermore, it can be seen the damping of the active power response changes depending on the selected inertia constant value. It can also be verified from Equation (3.9), where it can be seen that the damping ratio depends on both the inertia constant and the damping factor. Thus, the damping factor should be selected individually for each inertia constant to maintain the desired damping.

3.2.4 Evaluation of a load step event

A 10 % load step increase is applied to the test system to evaluate the response of the GF model in a realistic case. A pre-event static load of 100 MW is connected to the test system. After 5 seconds a 10 MW load is connected. The external grid is connected and configured to have an acceleration time constant of 10 s, and a frequency bias of 50 MW/Hz. The GF model is evaluated with two different inertia constants of 4 and 1. The damping factor is selected to have a slight underdamped response with a K_D of 200. The test result can be seen in Figure 3.15.

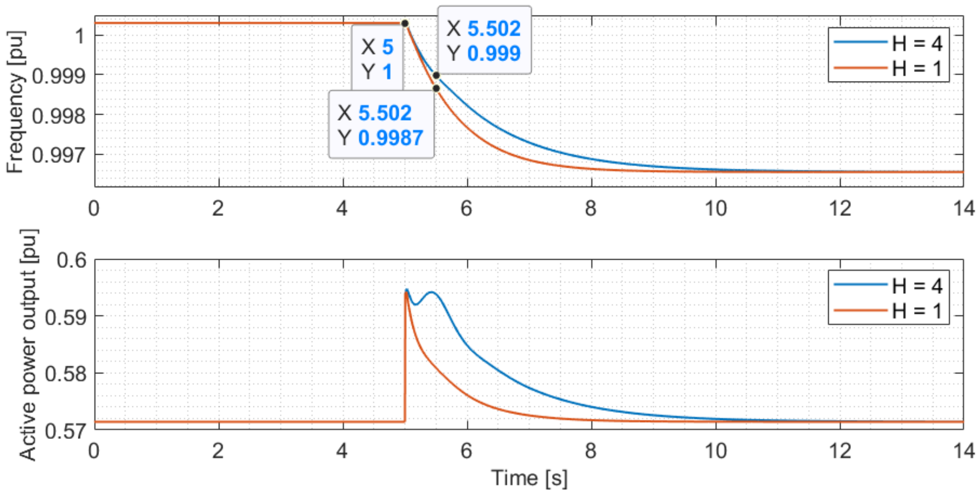

Figure 3.15: Evaluation of the GF model owing to a 10% load step increase with two different inertia constants of 4 and 1.

From Figure 3.15, it can be seen that the RoCoF is higher for the case with low inertia constant, which is as expected. Calculating the RoCoF based on a 500 ms time window, the RoCoF is found to be 0.1 Hz/s with H equal to 4 and 0.125 Hz/s with H equal to 1. Thus, the GF model can reduce the RoCoF, owing to a load step event.

The steady state frequency deviation due to the load step can be calculated from Equation (3.14). Note the frequency deviation from Equation (3.14) is converted to a pu value. [15]

$$\Delta f = \frac{-\Delta P_{Load}}{\beta} = \frac{-10MW}{50MW/Hz} = -0.004pu \tag{3.14}$$

Where β is the external system frequency bias. The steady state frequency deviation can be verified visually from Figure 3.15.

3.2.5 Evaluation of current limiter

The current limiter applied to the GF model is implemented to reduce the current output during fault scenarios. The current limiter is evaluated in Figure 3.16. A three-phase fault is applied to the test system at the busbar *PCC_GFC*, which is the high voltage connection point of the aggregated wind farm. The fault is applied for 200 ms. The fault event is simulated with and without the current limiter to evaluate the response.

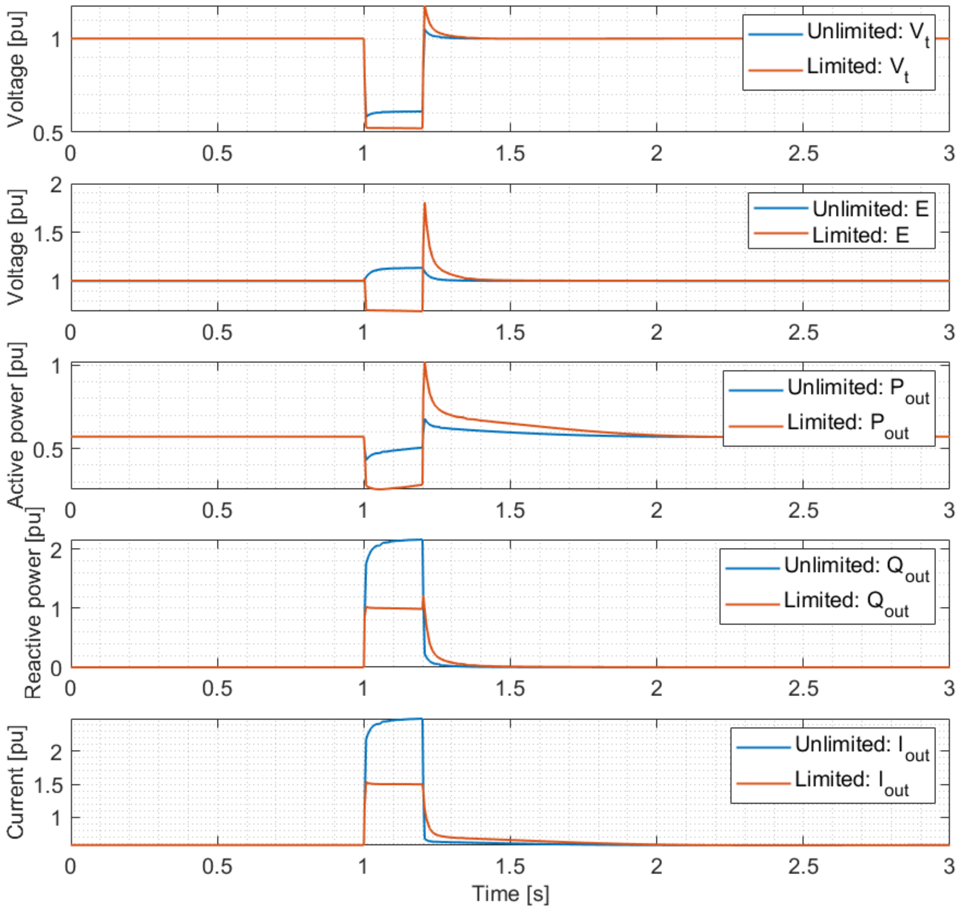

Figure 3.16: Evaluation of the current limiter in the GF model. A three phase fault is applied to the test system with and without the current limiter.

From Figure 3.16, it can be seen that the terminal voltage of the converter, V_t, drops to approximately 0.5 pu, when a limited current is considered. The converter terminal voltage for the unlimited current drop to approximately 0.6 pu. It higher retained voltage level, can be explained from the internal converter voltage, E, which is not constrained and hence will increase the reactive power output and restraint the voltage drop. From the unlimited current simulation, it can be seen that the current increases to almost 2.5 pu during the fault event. The high current is a result of the fault impedance. Opposite, it can be seen that the current is restrained at 1.5 pu, when the current limiter is enabled, which is the selected maximum allowed converter current for the GF model. The active power output of both simulation cases is decreased during the fault event as the voltage drops. Post fault, the active power output of the GF model increases close to instantaneously owing to the voltage recover post fault. The active power response from a WTG is typically ramped post fault to limit the mechanical stress on WTGs. However, a post-event active power limiter is not added to the GF model. [30] Furthermore, it should be noted that the selected maximum current of the GF model of 1.5 pu is beyond the typical maximum current rating of WTGs which is 1.1 to 1.2 pu [31]. Thus, the WTG converters are required to be up-scaled to oblige with the 1.5 pu current limit in the GF model.

3.3 Summary

In this chapter, it has been explained how a dynamic RMS model of an aggregated wind farm operating in grid forming mode can be implemented into DIgSILENT PowerFacory. The GF model was based on the VSM converter control concept, as explained in Section 2.4. The interface and control of each block of the GF model have been described. The response of the GF model was then evaluated in Section 3.2. It has been explained how the GF model response to different system events, including the effect of the properties, inertia constant and damping factor. Lastly, it has been shown how the current output of the GF model could be constrained during severe fault events to protect the converter from exceeding a maximum allowed current output.

Chapter 4

Comparison of the GF model to an SG and WTG model

In this chapter, the grid-forming WTG model described in Section 3.1 will be compared to a conventional SG and WTG model. It will be elaborated on how the GF model will support power system disturbances compared to SGs and WTGs. Therefore, an SG model and an aggregated WTG model have been implemented and setup in DIgSILENT PowerFactory together with the GF model from Chapter 3.

The SG model utilised in this analysis is a 210 MVA generator, where an excitation and governor controller is installed from PowerFactory's global dynamic library. The WTG model consists of 29, 6 MW WTGs, aggregated to one 174 MW model. The WTGs are installed based on PowerFactory's generic dynamic template library. The three models are connected to a test system, as displayed in Figure 4.1.

The parameters of the different elements in the test system in Figure 4.1 are summaries in Table 4.1. The listed values in pu are based on their rated values, besides the transmission lines, which is based on a base power of 175 MVA.

Table 4.1: Ratings and parameters of the different elements in Figure 4.1

Elements	V [kV]	S [MVA]	X [pu]	R [pu]
GF/WTG trafo	33/132	190	0.125	0.004
SG trafo	17/132	210	0.125	0.004
Line	132	-	0.049	0.005
External grid	132	Sk"_max = 3000	X/R =10	

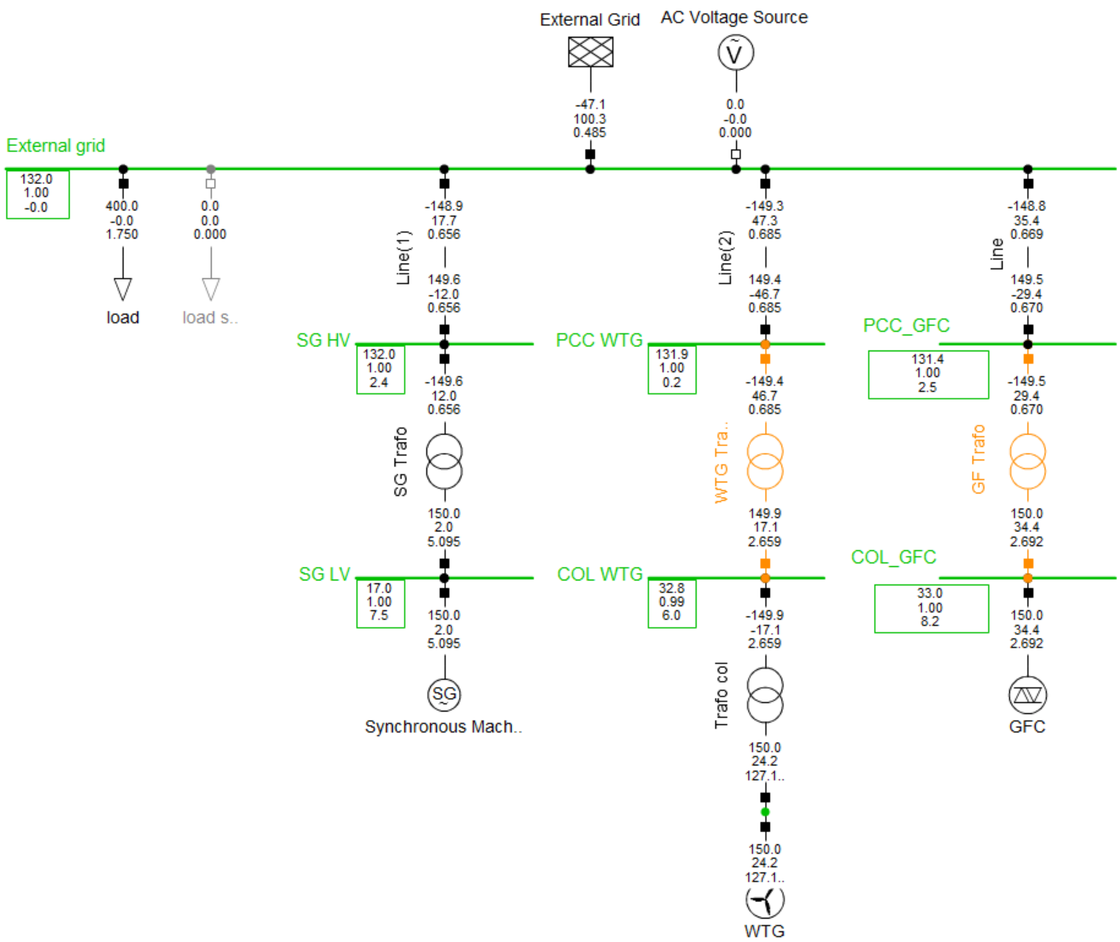

Figure 4.1: Screenshot of the test system setup in DIgSILENT PowerFactory with the three generators. From the left, the first generator displayed is the SG model, the second is the WTG model and the third is the GF model.

4.1 Comparison of ideal frequency step event

The response from the three generator models in Figure 4.1 will be evaluated in this section, owing to a frequency step event. A frequency step of 0.004 pu is applied to the AC voltage source displayed in Figure 4.1, which represent an ideal external system. The damping factor and inertia constant for the SG and GF unit are identical and selected to be, 12 and 4, respectively. Furthermore, the governor speed droop and frequency-droop controller is disabled for the SG and GF model. The response from the frequency event of the three-generation units can be seen in Figure 4.2. As can be seen from Figure 4.2,

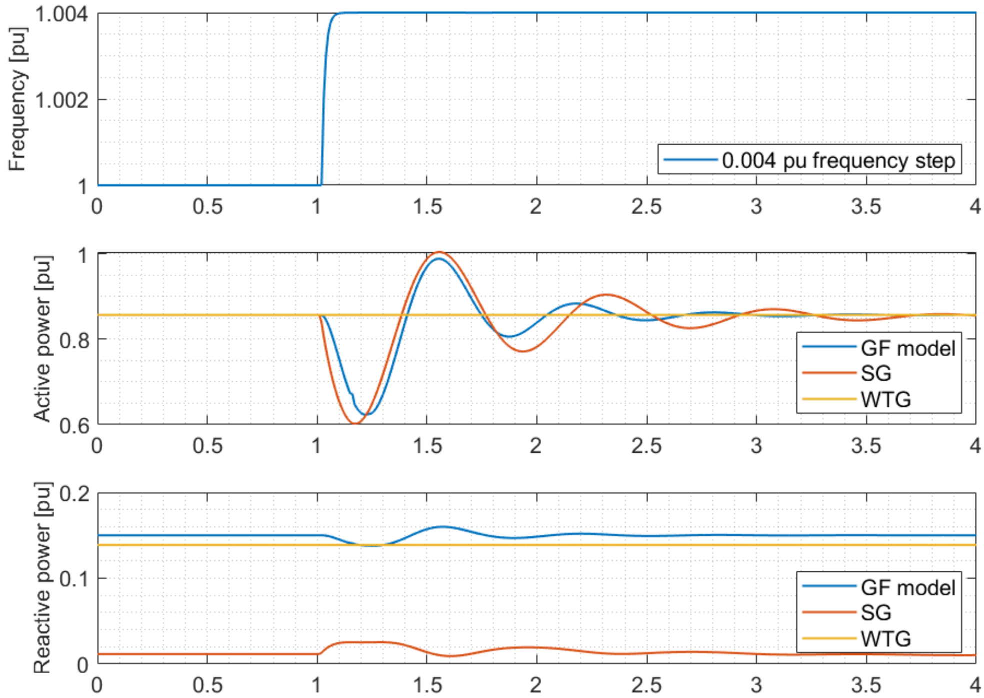

Figure 4.2: Comparison of the response of three-generation units installed in the test system owing to pseudo frequency step event of 0.004 pu.

the active power trend of the SG and GF model is highly comparable. However, the response from the SG is slightly faster and less damped than the GF model. The active power response from the WTG is unchanged during the disturbance as the WTG is controlled to inject a constant power. The reactive power response from the three units depends on the voltage regulator. A voltage droop regulator is utilised for the GF model and WTG where a constant voltage reference is applied for the SG. Thus, the reactive power contribution of the GF model and WTG is higher than the SG unit.

4.2 Comparison of the GF model to the SG model

4.2.1 Load step event

In this section, the GF model is compared to the SG model, where a 10% load step is applied. The external grid in Figure 4.1 is replaced with the AC voltage source. The external grid has a short circuit power of 3000 MVA, an acceleration time constant, T_a, of 10s and a frequency bias, β, of 150 MW/Hz. The droop gain in the governor and frequency-droop controller of the SG and GF model is set to 5%. The inertia constant is selected to be 4s for both the SG and GF model. The damping factor of the GF model is selected to be slightly underdamped with a K_D of 200, where the damping factor for the SG is selected to be 14. The damping factor of the SG is selected to obtain a damping ratio in the range of 0.1 - 0.2, which is the typical damping ratio of an SG [15][7]. A system load is stepped from 300 MW to 330 MW. The system frequency and active power contribution from the SG and GF model are displayed in Figure 4.3. As can

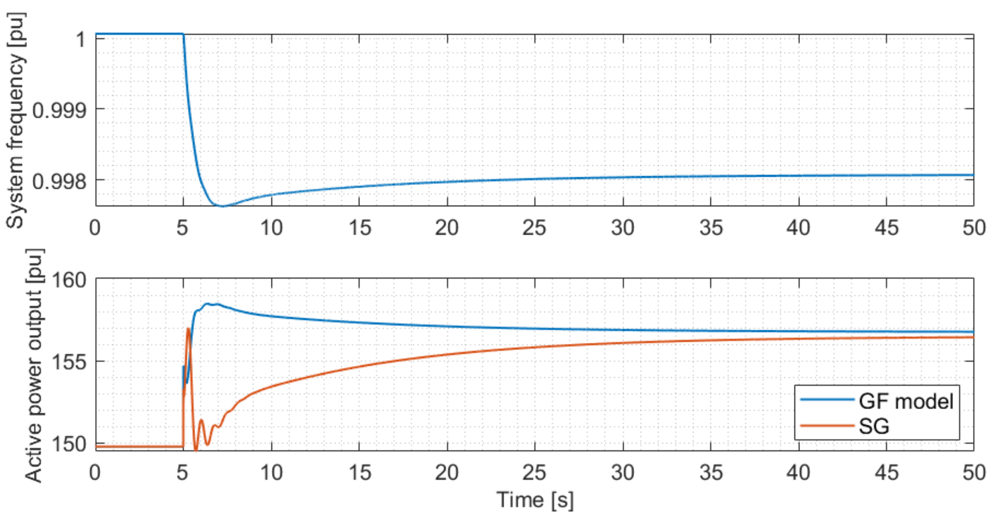

Figure 4.3: Comparison of the active power response of the SG and GF model in the test system owing to a 10% load step increase, where the frequency-droop controller in the GF model is unconstrained.

be seen from Figure 4.3, the active power response of the GF model is rapid with a fast settling time, whereas the active power response of the SG is slower with a long settling time. It can be explained from the governor time constants for the SG, which represents the real system delay of a conventional SG with the mechanical operation. Opposite, the GF model does not have any inherent time constants. However, depending on the dedicated power source utilised to increase the electrical power output owing to a load step, it can be necessary to implement a delay. I.e. if the additional power is drawn from a curtailed WTG, then the additional power can not be delivered instantaneously, as the WTG will need to operate the pitch system to increase the mechanical output power.

In Figure 4.4, the same test event is simulated, where a delay block is now added to the frequency-droop controller of the GF model, to represent the mechanical delay of an SG.As can be seen in Figure 4.4, the response of the GF model is now slower and closer to the SG.

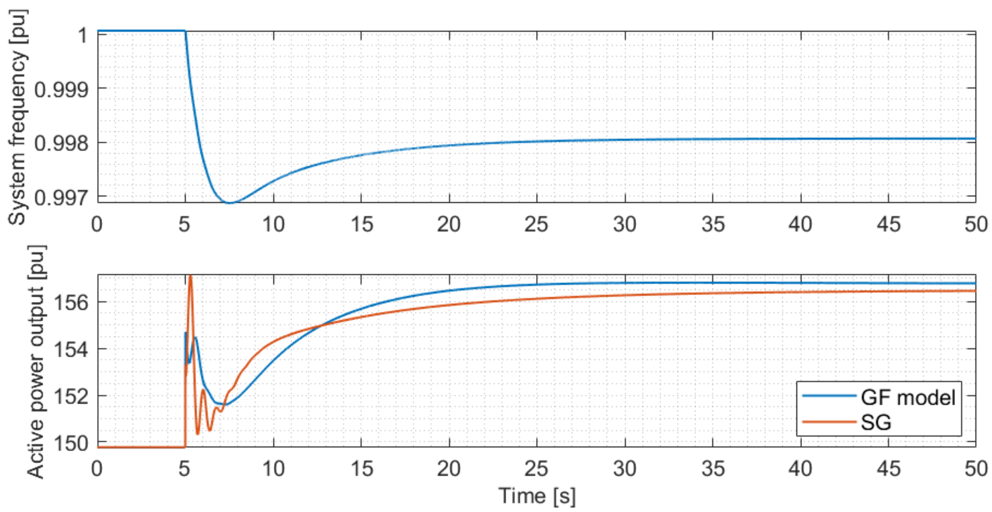

Figure 4.4: Comparison of the active power response of the SG and GF model in the test system owing to a 10% load step increase, where the response from the frequency-droop controller in the GF model is delayed.

As explained in Section 3.1, the frequency-droop controller is not an inherent feature of a GFC. Thus, the effect of disabling the frequency-droop controller for the GF model is displayed in Figure 4.5.

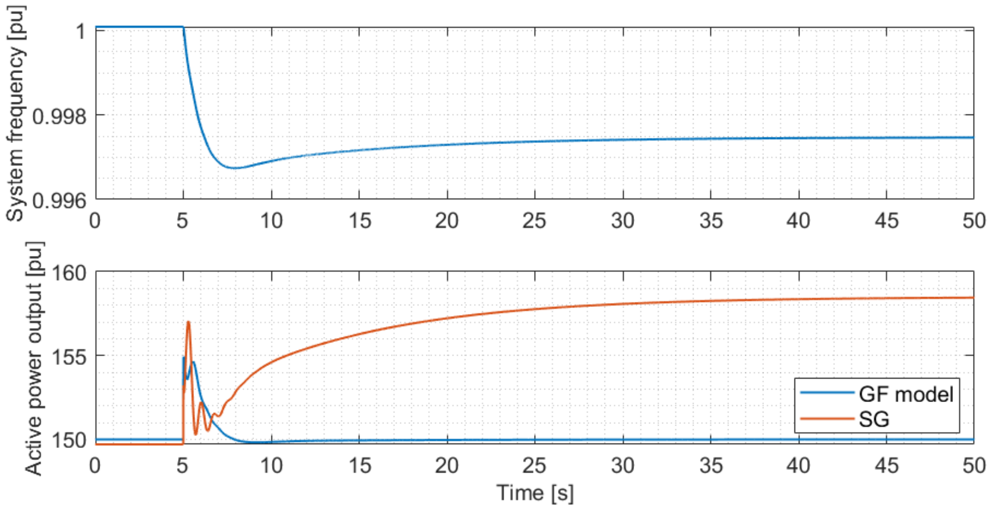

Figure 4.5: Comparison of the active power response of the SG and GF model in the test system owing to a 10% load step increase, where the frequency-droop controller in the GF model is disabled.

As can be seen from Figure 4.5, the GF model is still contributing to minimising the RoCoF. However, after the system disturbance, the GF model returns to the pre-event active power set-point.

The RoCoF and frequency nadir for the three cases are summarised in Table 4.2.

Table 4.2: Summary of the RoCoF and frequency nadir for the three simulation cases.

	RoCoF [Hz/s]	Frequency nadir [pu]
Case 1 (Figure 4.3)	0.15	0.9976
Case 2 (Figure 4.4)	0.15	0.9969
case 3 (Figure 4.5)	0.15	0.9967

From Table 4.2, it can be concluded that a fast frequency-droop controller without delay will reduce the frequency nadir. Moreover, it can be concluded that the RoCoF is unchanged for the three cases. That is the case, as it is only the frequency-droop controller which has been altered.

4.2.2 Short circuit event

In this section, a fault event is applied to both the SG and GF model, to compare the short circuit current supplied by the two generators.

The point of common coupling (PCC) for a wind farm is typically referring to the high voltage terminal of the park transformer. The PCC is the location in the collector network where the TSO specifies the requirements for a grid-connected unit. Hence, the point, i.e. where the short circuit current contribution from WTGs is specified. Thus, a bolted fault is applied for 150 ms on the high voltage terminal of the GF models park transformer, which is referred to as bus *PCC_GFC* in Figure 4.1. A similar event is repeated for the SG, where a bolted fault is applied for 150 ms on the high voltage terminal of the SGs transformer, which is referred to as bus *SG_HV* in Figure 4.1. The results from the two simulations are displayed in Figure 4.6.

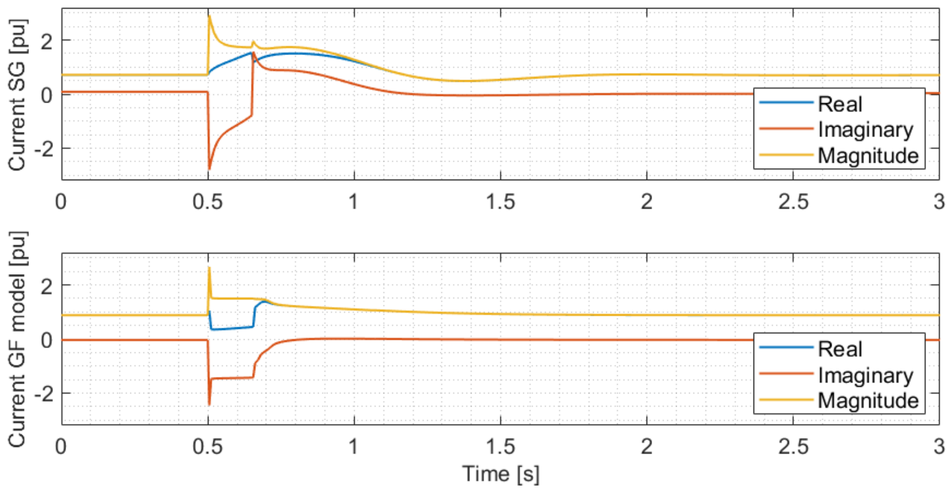

Figure 4.6: Comparison of short circuit current for the SG and GF model due to a bolted fault applied at the high voltage terminal of their transformers.

From Figure 4.6, it can be seen that the short circuit current from the SG initially reaches approximately 3 pu current, which is due to the sub-transient and transient impedance of the SG. However, the steady-state current settles at about 1.7 pu.

The short circuit current capacity of an SG is high, as explained in Section 2.5, in the range of 5-8 pu. However, based on the bolted fault applied at the high voltage side of the transformer, a short circuit contribution of approximately 1.7 pu is supported by the SG. It can be explained, from the high serial impedance of the transformer, which will increase the impedance seen by the SG and hence lower the output current form the SG.

The short circuit current from the GF model indicates an initial spike, which ideally should be eliminated from the current limiter in the model, however, the steady-state short circuit current settles at 1.5 pu. The 1.5 pu current limits, is chosen based on National Grid's recommendation for GFC, as explained in Section 2.5.

The steady-state short circuit current contribution from the SG in Figure 4.6 is approximately 0.2 pu higher than the short circuit current contribution from the GF model. Hence, the steady-state short circuit contribution from the two generators are adjacent, even though the SG's short circuit current capability is substantially larger.

4.3 Evaluation of system frequency for various generation setup

In this section, the three-generation units shown in Figure 4.1 are setup in various test cases to evaluated how the system frequency is influenced, based on a 10% load step.

The three-generation units shown in the test system in Figure 4.1 are duplicated. Thus, two of each generation unit is connected to the test system now. Base on the test system is the following test cases set up.

- 100% SG connected
- 50% SG & 50% WTG connected
- 100% WTG connected
- 50% SG & 50% GF model connected
- 100% GF model connected

e.g. 100% SG connected, implies two SG models is connected to the test system each with a 150 MW production. 50% SG & 50% WTG connected, implies one SG model and one WTG model is connected to the test system, each with a production of 150 MW.

The droop gain in the governor and frequency-droop controller of the SG and GF are both set to 5%, and no delay is applied to the GF model's frequency-droop controller.

The configuration of the external grid in the test system is changed to evaluate the influence of the external grid. Four configurations of the external grid are therefore tested. The configurations are the following:

- Case 1) has a T_a of 10s and a β of 150 MW/s (same settings as in Section 4.2)
- Case 2) has a T_a of 1s and a β of 150 MW/s
- Case 3) has a T_a of 10s and a β of 15 MW/s
- Case 4) the external grid is disconnected (The test system is in island mode)

Analysis of case 1:
The system frequency owing to the load step, for the five different percentages of generation units connected to the test system, is displayed in Figure 4.7. The external grid is configured as case one. The lowest steady-state system frequency for the test system is

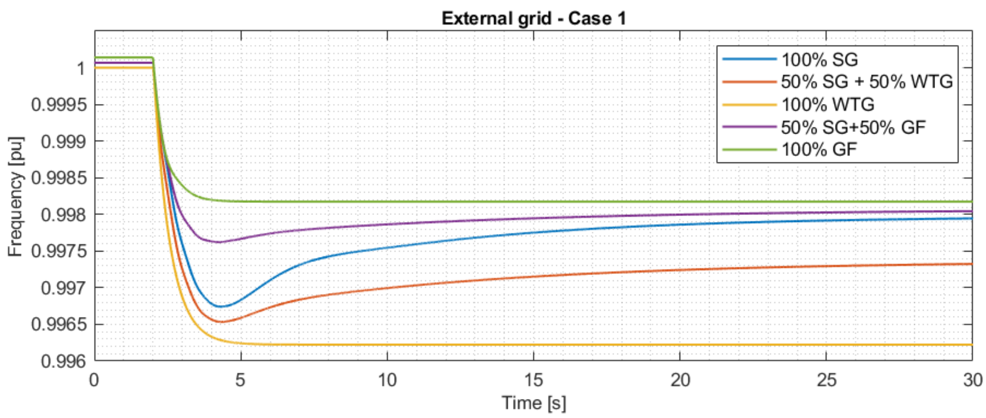

Figure 4.7: Comparison of the system frequency response for five different percentages of generation units connected with an external grid settings of case one.

obtained, when the test system is 100% WTG connected. Opposite, the highest steady-state system frequency for the test system is obtained when the test system is 100% GF connected. It can be explained from the fast frequency-droop controller of the GF model. The RoCoF and frequency nadir for the five different simulations in Figure 4.7 are summarised in Table 4.3.

Analysis of case 2:
Changing the external grid to case two, with a T_a of 1s, and repeating the same simulations, the corresponding system frequency is obtained as displayed in Figure 4.8. From

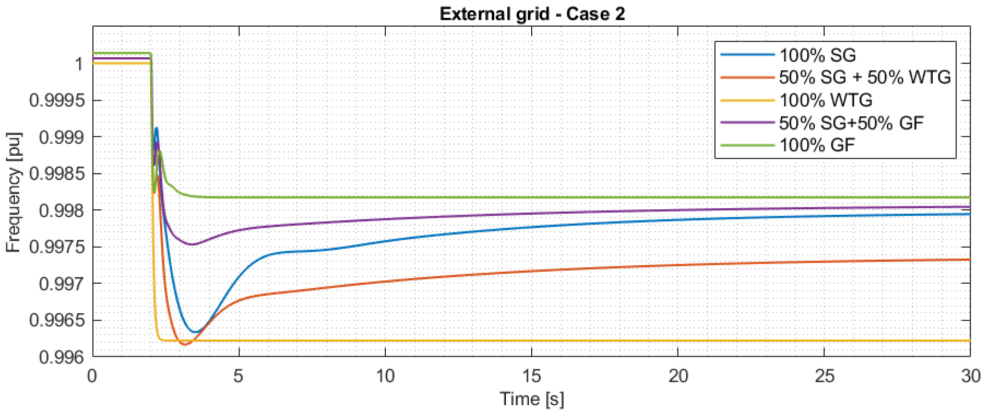

Figure 4.8: Comparison of the system frequency response for five different percentages of generation units connected with an external grid settings of case two.

Figure 4.8, it can be seen that the system frequency trends are similar to Figure 4.7. However, the frequency nadir is lowered. Furthermore, as the external system is made weaker with a lower T_a, oscillations are observed from the generating units. The RoCoF and frequency nadir for the five different simulations in Figure 4.8 are summarised in Table 4.3.

Analysis of case 3:

The external grid is then changed to case three, with a T_a of 10s and β of 15 MW/s and the simulations are repeated. The system frequency is displayed in Figure 4.9. As can

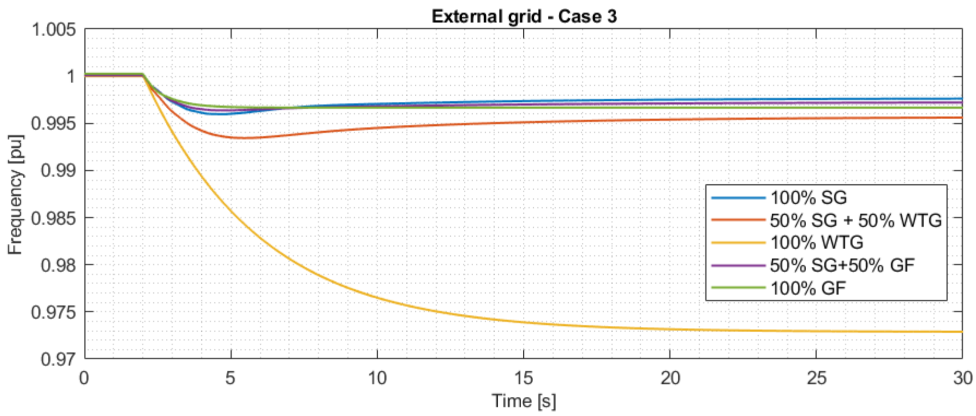

Figure 4.9: Comparison of the system frequency response for five different percentages of generation units connected with an external grid settings of case three.

be seen from Figure 4.9, the new equilibrium steady-state system frequency post-event is reached slower than in Figure 4.8. Moreover, the new equilibrium system frequency is lower. It can be seen that the case with 100% WTG unit connected, the frequency decreases slowly towards a frequency of 0.97 pu as the frequency bias is low. The RoCoF and frequency nadir for the five different simulations in Figure 4.9 are summarised in Table 4.3.

Analysis of case 4:
The external grid is now disconnected, and the test system is operated in island mode. The same simulations for the generation setup are repeated. The system frequency is displayed in Figure 4.10 As it can be seen from Figure 4.10, the system frequency for a

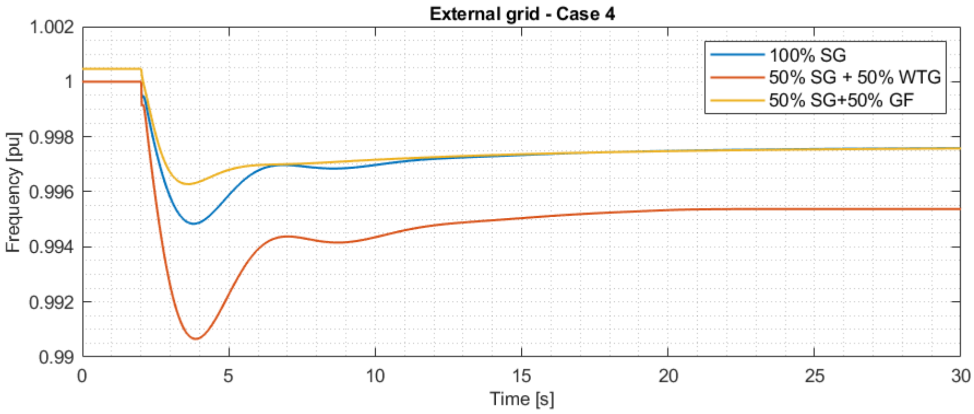

Figure 4.10: Comparison of the system frequency response for five different percentages of generation units connected when the external grid is disconnected.

generation setup with 100% WTG and 100% GF is not displayed. It is the case, as it was not possible to run the simulations in PowerFactory. The 100% WTG setup can not be operated in island mode as the WTG is based on grid-following control. Thus, a stable AC source is required to connect the WTG model. However, it was also found that it was not possible to run the test system based on a 100% generation from the GF model. The RoCoF and frequency nadir are summarised in Table 4.3.

The RoCoF values displayed in Table 4.3 is calculated based on a 500ms measuring window. From Table 4.3, it can be observed as expected, that the acceleration time constant of the external grid has a significant impact on the RoCoF and approximately no effect on the frequency nadir. Oppositely, it can be observed that the frequency bias has a larger effect on the frequency nadir values.

Table 4.3: Summary of the RoCoF and frequency nadir for the five different set-up cases of the generation units together with the four cases of the external grid settings.

	RoCoF [Hz/s]				Frequency nadir [pu]			
External grid case:	1	2	3	4	1	2	3	4
100 % SG	0.14	0.23	0.15	0.24	0.9967	0.9964	0.9960	0.9948
50% SG + 50% WTG	0.17	0.312	0.21	0.42	0.9965	0.9962	0.9934	0.9907
100% WTG	0.22	0.4	0.31	-	0.9962	0.9962	0.9729	-
50% SG + 50% GF	0.13	0.22	0.16	0.19	0.9976	0.9976	0.9663	0.9963
100% GF	0.13	0.16	0.19	-	0.9982	0.9982	0.9966	-

ENTSO-E recommend a minimum RoCoF withstanding capability for grid-connected units of 2 Hz/s [32]. Hence, it can be concluded that the RoCoF created from the load step event for the test system will not provoke a critical power system condition, where generation units are allowed to disconnect. However, lowering the external grid strength, the power system does become more fragile and larger RoCoF, and frequency nadir are observed. Thus, the contribution from the external grid is essential to consider.

Furthermore, from Table 4.3, it can be seen that the test case with 100% WTG connected has the highest RoCoF and the lowest frequency nadir for all four cases of the external grid setup. It is as anticipated since the WTG is not providing any inertia or frequency support.

Moreover, it can be seen that the cases with either 100% SG or 100% GF have the lowest RoCoF. However, it can be concluded, replacing the SG model with the GF model, the RoCoF and frequency nadir can be significantly reduced compared to replacing the SG model with the WTG model. Furthermore, it is found that the GF model can reduce the frequency nadir compare to the SG model. It can be explained from the fast frequency-droop controller in the GF model.

4.4 Summary

In this chapter, it was analysed how the grid forming WTG model developed in Chapter 3 can support a power system when subjected to system disturbances. The evaluation has been achieved by comparing the grid forming WTG model to the reference response from a conventional SG and WTG model.

A pseudo frequency step event was applied to the test system setup in PowerFactory, where it was found that the trends of the GF model are highly comparable to an SG. However, the response of the GF model was found to be 0.05 s slower than the SG model and had a higher damping response. Thus, it can be concluded that a trade-off exists between the response time and damping ratio.

The response of the frequency-droop controller of the GF model was then compared to the governor controller of the SG. It was found that the frequency-droop controller of the GF model is much faster than the governor controller of the SG. Moreover, it was concluded, that the fast frequency-droop controller in the GF model can reduce the frequency nadir compared to an SG.

Various generation setups were then analysed for the test system, where it was concluded that the strength of the external grid has a considerable influence on the RoCoF and frequency nadir. Furthermore, it was concluded that the GF model could improve the RoCoF and frequency nadir compared to conventional WTGs, which showed no support. The GF model showed better results in reducing the frequency nadir compared to the SG model. Moreover, it was found that if the test system was set up with 100% GF connected, it could not be operated in island mode. However, the GF model could operate island mode if the SG model was installed at the same time.

Chapter 5

Discussion

This chapter is written to interpret and evaluate some of the decisions and results presented in the project.

The development of the dynamic grid-forming WTG model in Chapter 3, was based on the GFC control concept referred to as, virtual synchronous machine (VSM). The model was based on a direct voltage control of the static generator block in PowerFactory. Thus, a current limiting algorithm was added to the GF model to restrain high current demands. Nevertheless, the VSM method was selected as the desired characteristic to represent an aggregated wind farm model in the RMS domain could be obtained. However, this particular method is only presenting one concept of capturing the GFC characteristic, as explained in Section 2.4.

As demonstrated in Section 3.2 and Section 4.2, the GF WTG model was able to limit the short circuit current during a fault event. However, the post fault active power was not limited. Thus, the post-event active power recovers close to instantaneously. It will be an unreal behaviour for a WTG, as an immediate power increase will have a large mechanical load, which is typically prohibited for WTGs. Thus an active power ramp is normally applied after a fault event.

The dynamic grid-forming WTG model makes use of a PLL block in PowerFactory to measure the system frequency. The measured system frequency is used as a reference to determine system frequency disturbances. Thus, the PLL block is not utilised to synchronise the power converter to the AC grid. In other literature's, a nominal synchronous frequency is used instead, to make the system frequency measurement redundant [33][29]. It could also explain why it was not possible to operate the test system in Chapter 4 in island mode with 100% GF unit connected. However, this was not further investigated.

The dynamic grid-forming WTG model was compared to a conventional SG and WTG model in Chapter 4. The GF model showed to be slightly slower and more damped than the SG model in the ideal comparison even though the same damping factor was applied in both units. However, considering the ideal evaluation of the GF model in Section 3.2, a similar trend was found, that a mismatch existed between the simulated damping response and the calculated damping ratio. Furthermore, the SG model implemented in PowerFactory has a higher level of details compared to the developed grid-forming WTG model.

In Section 4.2.1, the governor controller of the SG was compared to the frequency-droop controller in the GF model. The reaction time of the GF model showed to be significantly faster. However, no delay was considered for the GF models frequency-droop controller. Thus, a straight comparison can not be made, as a WTG will also encounter some additional delays as an SG. The delay time will depend on the specific setup for the WTGs operating in grid forming mode. I.e. if the power from a WTG is curtailed to gain a power headroom, and the system frequency then decreases and hence the power reference increases. The pitch system in the WTG then needs to be activated to harvest the additional power required. This operation will have a mechanical response time, which needs to be considered for the frequency-droop controller in the GF model.

In Section 4.2.2, the short circuit current contribution from the SG and GF model was compared. It was found that the steady-state short circuit current from the SG was 0.2 pu higher than the limited short circuit current from the GF model. However, the sub-transient and transient short circuit current from an SG is essential to consider, as the setting of protection relays are typically based on these values, since relay times range from 1 to 2 cycles [15]. Thus, caution should be made when evaluating the short circuit contribution from the GF model with an SG.

In Section 4.3 on the RoCoF and frequency nadir were evaluated. The RoCoF was calculated based on a 500 ms measuring window. However, the measuring window can have a significant effect on the RoCoF value. The calculated RoCoFs values in Table 4.3 with the external grid of case one, are re-calculated based on a 100 ms measuring window and compared in Table 5.1.

Table 5.1: Difference in RoCoF based on a 500 ms and 100 ms measuring window

External grid	RoCoF [Hz/s]		Difference
(Case 1)	500 ms	100 ms	[%]
100 % SG	0.14	0.19	26
50% SG + 50% WTG	0.17	0.23	26
100% WTG	0.22	0.29	24
50% SG + 50% GF	0.13	0.16	19
100% GF	0.13	0.17	23

From Table 5.1, it can be observed that a significant difference exists for the two measuring windows. The most substantial difference in the RoCoF value is found to be 26%. Thus, the measuring window used to determine the RoCoF is vital to consider. E.g. a large number of distributed grid-connected generators utilised RoCoF relays for protection. Hence, detecting a wrong RoCoF can lead to unintended cascade tripping of distributed generators, and thus deteriorate the power system condition further. [34][7]

Chapter 6

Conclusion and Future work

Conclusion

This section will present and conclude on the essential findings presented in the project.

From Section 2.4, the essential characteristics of a GFC were presented. It was described, that a GFC should behave like a voltage source behind an impedance to fulfil ENTSO-E definition of a GFC. It implies that the current drawn from the grid-forming unit should be determined from the load and network condition.

In Chapter 3, a dynamic grid-forming WTG model was developed. The GF model was developed to represent an aggregated wind farm. The GFC control concept, VSM, was utilised to obtain the GF model in PowerFactory. A voltage regulator was used to control the internal voltage magnitude of the converter, where the virtual rotor angle of an SG was obtained from modelling the swing equation. The virtual rotor angle was then used to obtain the real and imaginary voltage vector components, which were used as input signals to the voltage source in PowerFactory.

The grid-forming WTG model was evaluated based on various test cases, where it was found the GF model performed as anticipated. By changing the inertia constant and damping factor in the GF model, it was possible to change the system support of the GF model.

From Section 3.2, it was concluded, that the GF model can provide fault current in relation to fault impedance. It implies the GF mode represents a true voltage source behind an impedance, which ENTSO-E has described, as a defining characteristic of a grid forming unit as described in Section 2.4.

The GF model was implemented in a setup with an SG and a WTG model in Power-Factory, to compare the power system support from the three units. It was concluded that the GF model was able to operate in parallel with other power units. Hence, being able to synchronise with other grid forming units. However, it was found that it was not possible to operate the GF model as a standalone unit in island mode. Nevertheless, it was possible to operate the GF model in island mode if the SG model was added.

Furthermore, from comparing the GF model to the SG in Section 4.2, it was found that the GF model can outperform the SG to some extent but was restricted in others. The GF model presents more flexibility compared to an SG, as, e.g. the inertia contribution and damping factor are defined from software and can, therefore, be selected freely. Yet, the hardware of the GF model needs to support the selected parameters. Oppositely, the SG's inertia contribution and damping factor are defined from the physical design of an SG and thus presents less flexibility. Nevertheless, the GF model is subjected to hardware limitations, and thus the short circuit current contribution is limited. Furthermore, the frequency-droop controller in the GF model will also introduce some limitations, as the GF model will need sufficient energy storage to allow such service. However, this was not further addressed in the report.

From Section 4.3, it was concluded, that the GF model could improve the RoCoF and frequency nadir compared to conventional WTGs. It was found, that replacing the SG model with the GF model, the RoCoF and frequency nadir can be significantly reduced compared to replacing the SG model with the WTG model. Furthermore, it was concluded that the GF model could reduce the frequency nadir compare to the SG model.

Future work

From working on this topic, some areas have emerged which have not been addressed in this project. These areas will be presented as recommendations for future work.

- The system disturbances analysed in the different test cases in this project cover only a limited range of possible tests. Thus, future test cases are required to broaden the understanding of the GF models influence on power systems. E.g. scale the test system to a 9 or 13 busbar system, which are often used in power system studies.
- Investigate the potential of operating the GF model exclusively in an island mode. It will enlarge the understanding of the GF model and further evaluate the substi-

tution of SG.

- The GF model implemented in this project does not consider the limited available power of a WTG. However, applying GFC control to a WTG, a relevant aspect would be to consider the available power limitations and address the need for dedicated storage.
- A current limiter is added to the GF model in this project. However, it has not been addressed how the replacement of SG's sub-transient and transient current with a steady-state current from the GF model, will affect the protection in power systems. Thus, it will be relevant to investigate how the conventional protection relays in power systems will need to be changed to oblige with a more extensive penetration of GFC based power units.

Bibliography

[1] ENTSO-E, *High penetration of power electronic interfaced power sources*, 2017.

[2] ENTSO-E Technical Group, *High penetration of power electronic interfaced power sources and the potential contribution of grid forming converters*, 2019.

[3] P. Brogan, T. Knueppel, D. Elliott, and N. Goldenbaum, “Experience of grid forming power converter control”, 2018.

[4] H. Urdal, R. Ierna, J. Zhu, C. Ivanov, and A. Dahresobh, “System strength considerations in a converter dominated power system”, *IET Renewable Power Generation*, vol. 9, no. 1, pp. 10–17, 2015.

[5] IEEE power & energy magazine, *Grid-forming inverters*, 2019.

[6] H. Urdal, R. Ierna, and A. Roscoe, “Stability challenges & solutions for power systems operating close to 100% penetration of power electronic interfaced power sources: Exchange of experience between hybrid and major power systems”, May 2018. [Online]. Available: `http://hybridpowersystems.org`.

[7] A. Roscoe, M. Yu, A. Dyśko, C. Booth, R. Ierna, J. Zhu, and H. Urdal, “A vsm (virtual synchronous machine) convertor control model suitable for rms studies for resolving system operator / owner challenges”, Nov. 2016.

[8] MIGRATE, *Migrate – massive integration of power electronic devices*. [Online]. Available: `https://www.h2020-migrate.eu/_Resources/Persistent/fc20f34591b33833312ddad41b714f50015ba626/MIGRATE_folder.pdf`.

[9] IEEE power & energy magazine, *Paving the way: A future without inertia is closer than you think*, 2017.

[10] D. Pattabiraman, R. H. Lasseter, and T. M. Jahns, “Comparison of grid following and grid forming control for a high inverter penetration power system”, *2018 IEEE Power & Energy Society General Meeting PESGM*, pp. 1–5, 2018.

[11] GE Reports, *Ge researchers developing advanced pv inverter technology to support more reliable, resilient solar grid integration*. [Online]. Available: https://www.genewsroom.com/press-releases/ge-researchers-developing-advanced-pv-inverter-technology-support-more-reliable?fbclid=IwAR2XoyK54v2Lbke9Qbaj1LgFzs9oxnJlAreBhb3zc0Eb602UkJDkcSj_uok.

[12] SMA, *Battery inverters*. [Online]. Available: https://www.sma.de/en/products/battery-inverters.html.

[13] A. Roscoe, P. Borgan, D. Elliott, T. Knuppel, I. Gutierrez, J. P. Campion, and R. D. Silva, "Practical experience of operating a grid forming wind park and its response to system events", 2019.

[14] J. Machowski, *Power system dynamics : stability and control /*, Elektronisk udgave. -2nd ed. Chichester, U.K: Wiley, 2008, ISBN: 9780470725580.

[15] P. Kundur, *Power system stability and control*, 1. ed. McGraw-Hill Education, 1994.

[16] *Modeling and Modern Control of Wind Power*. Chichester, UK: John Wiley & Sons, Ltd, 2017, ISBN: 9781119236269.

[17] *Variable-Speed Wind Energy Systems with Synchronous Generators*. John Wiley & Sons, Ltd, 2011, ch. 9, pp. 275–316, ISBN: 9781118029008. DOI: 10.1002/9781118029008.ch9. [Online]. Available: https://onlinelibrary.wiley.com/doi/abs/10.1002/9781118029008.ch9.

[18] J. Rocabert, A. Luna, F. Blaabjerg, and P. Rodríguez, "Control of power converters in ac microgrids", *IEEE Transactions on Power Electronics*, vol. 27, no. 11, pp. 4734–4749, Nov. 2012, ISSN: 1941-0107. DOI: 10.1109/TPEL.2012.2199334.

[19] R. Ierna, A. Johnson, B. Marshall, H. Urdal, C. Li, M. Sumner, and A. Egea-Àlvarez, "Dispatching parameters, strategies and associated algorithm for vsm (virtual synchronous machines) and hgfc (hybrid grid forming convertors)", English, 19th Wind Integration workshop ; Conference date: 16-10-2019 Through 18-10-2019, Oct. 2019.

[20] S. D'Arco and J. A. Suul, "Virtual synchronous machines — classification of implementations and analysis of equivalence to droop controllers for microgrids", in *2013 IEEE Grenoble Conference*, Jun. 2013, pp. 1–7. DOI: 10.1109/PTC.2013.6652456.

[21] M. Yu, A. J. Roscoe, C. D. Booth, A. Dysko, R. Ierna, J. Zhu, N. Grid, and H. Urdal, “Use of an inertia-less virtual synchronous machine within future power networks with high penetrations of converters”, in *2016 Power Systems Computation Conference (PSCC)*, Jun. 2016, pp. 1–7. DOI: 10.1109/PSCC.2016.7540926.

[22] M. Yu, A. Dyśko, A. Roscoe, C. Booth, R. Ierna, H. Urdal, and J. Zhu, “Effects of swing equation-based inertial response (sebir) control on penetration limits of non-synchronous generation in the gb power system”, in *International Conference on Renewable Power Generation (RPG 2015)*, Oct. 2015, pp. 1–6. DOI: 10.1049/cp.2015.0388.

[23] I. Erlich, A. Korai, T. Neumann, M. Koochack Zadeh, S. Vogt, C. Buchhagen, C. Rauscher, A. Menze, and J. Jung, “New control of wind turbines ensuring stable and secure operation following islanding of wind farms”, *IEEE Transactions on Energy Conversion*, vol. 32, no. 3, pp. 1263–1271, Sep. 2017, ISSN: 1558-0059. DOI: 10.1109/TEC.2017.2728703.

[24] ENTSO-E, *Commission regulation (eu) 2016/631*. [Online]. Available: https://eur-lex.europa.eu/legal-content/EN/TXT/?uri=OJ:JOL_2016_112_R_0001#d1e1572-1-1.

[25] R. Ierna, S. Pholboon, M. Sumner, and C. Li, “Vsm (virtual synchronous machine) control system design, implementation, performance, models and possible implications for grid codes”, 2019.

[26] nationalgridESO, *Gc0100 annex 6- fast fault current injection supporting documents*. [Online]. Available: https://www.nationalgrideso.com/codes/grid-code/modifications/gc0100-eu-connection-codes-gb-implementation-mod-1.

[27] DIgSILENT GmbH, *Digsilent powerfactory version 2018 user manual*.

[28] E. Muljadi, S. Pasupulati, A. Ellis, and D. Kosterov, “Method of equivalencing for a large wind power plant with multiple turbine representation”, in *2008 IEEE Power and Energy Society General Meeting - Conversion and Delivery of Electrical Energy in the 21st Century*, 2008, pp. 1–9.

[29] L. Harnefors, M. Hinkkanen, U. Riaz, F. M. M. Rahman, and L. Zhang, “Robust analytic design of power-synchronization control”, *IEEE Transactions on Industrial Electronics*, vol. 66, no. 8, pp. 5810–5819, 2019.

[30] I. Erlich, F. Shewarega, S. Engelhardt, J. Kretschmann, J. Fortmann, and F. Koch, "Effect of wind turbine output current during faults on grid voltage and the transient stability of wind parks", in *2009 IEEE Power Energy Society General Meeting*, 2009, pp. 1–8.

[31] M. G. Taul, X. Wang, P. Davari, and F. Blaabjerg, "Current limiting control with enhanced dynamics of grid-forming converters during fault conditions", *IEEE Journal of Emerging and Selected Topics in Power Electronics*, vol. 8, no. 2, pp. 1062–1073, 2020.

[32] ENTSO-E, *Rate of change of frequency (rocof) withstand capability entso-e guidance document for national implementation for network codes on grid connection*, 2017.

[33] L. Lu, Ö. Göksu, and N. Cutululis, "Power angle small-signal stability analysis of grid-forming wind turbine inverter based on vsm control", English, in *Proceedings of the 18th wind integration workshop*, 2019. DOI: 10.5281/zenodo.3533020. [Online]. Available: http://windintegrationworkshop.org/.

[34] M. Rezkalla, M. Pertl, and M. Marinelli, "Electric power system inertia: Requirements, challenges and solutions", English, *Electrical Engineering*, vol. 100, no. 4, pp. 2677–2693, 2018, ISSN: 0948-7921. DOI: 10.1007/s00202-018-0739-z.